this pathway by expressing dnStat3 in cardiomyocytes almost abolished the protective effects of G-CSF on cardiac remodeling after myocardial infarction. In addition, there was no difference in the effects of G-CSF on mobilization and cardiac homing of bone marrow cells, expansion of cardiac stem cells, and proliferation of cardiomyocytes between wild-type and dnStat3-Tg mice. The beneficial effects of G-CSF and stem cell factor on the infarcted heart has been described, but no evidence indicating that G-CSF induced cardiac homing of bone marrow cells in the infarcted heart has been shown[1]. In this study, we found favorable effects of G-CSF on the infarcted heart as early as 1 week after the treatment even though cardiac homing of bone marrow cells was not increased. Thus, we conclude that increased cardiac homing of bone marrow cells cannot account for improved function of the infarcted heart after G-CSF treatment.

The JAK-STAT pathway has been shown to induce various angiogenic factors besides antiapoptotic proteins[20,21]. The number of endothelial cells in the border zone was increased by G-CSF through Stat3 activation in cardiomyocytes. Consistent with this, we noted that G-CSF induces cardiac expression of angiogenic factors *in vitro* and *in vivo*, which appears to be mediated by cardiac Stat3 activation (M.H., Y.Q., H.T., T.M. & I.K., unpublished data). Moreover, we observed that the majority of apoptotic cells in the infarcted hearts was endothelial cells and that endothelial apoptosis was significantly inhibited by G-CSF treatment in wild-type mice but not in dnStat3-Tg mice (**Fig. 4a** and M.H., T.M. & I.K., unpublished data). Thus, activation of this pathway in cardiomyocytes by G-CSF may also promote angiogenesis and protect against endothelial apoptosis by producing angiogenic factors, resulting in the further prevention of cell death of cardiomyocytes and cardiac remodeling after myocardial infarction. The results in this study provide new mechanistic insights of the G-CSF therapy on infarcted hearts.

METHODS

For further details, please see **Supplementary Methods** online.

Cell culture. Cardiomyocytes prepared from ventricles of 1-d-old Wistar rats[27] were plated onto 60-mm plastic culture dishes at a concentration of 1×10^5 cells/cm^2 and cultured in Dulbecco modified Eagle medium (DMEM) supplemented with 10% fetal bovine serum (FBS) at 37 °C in a mixture of 95% air and 5% CO_2. The culture medium was changed to serum-free DMEM 24 h before stimulation. Generation and infection of recombinant adenovirus were performed as described[28].

Percoll enrichment of adult mouse cardiomyocytes and noncardiomyocytes. Adult mouse cardiomyocytes were prepared from 10-week-old C57BL/6 male mice according to the Alliance for Cellular Signaling protocol. We also prepared cardiomyocytes and noncardiomyocytes from myocardial infarction-operated or sham-operated C57BL/6 male mice. After digestion, cells were dissociated, resuspended in differentiation medium and loaded onto a discontinuous Percoll gradient. Cardiomyocytes or noncardiomyocytes were separately collected as described previously[29] and subsequently washed with 1 × phosphate-buffered saline for RT-PCR.

RNA extraction and RT-PCR analysis. Total RNA from adult mice cardiomyocytes was isolated by the guanidinium thiocyanate-phenol chloroform method. A total of 4 μg RNA was transcribed with MMLV reverse transcriptase and random hexamers. The cDNA was amplified using a mouse *Csf3r* exon 15 forward primer (5′-GTACTCTTGTCCACTACCTGT-3′) and an exon 17 reverse primer (5′-CAAGATACAAGGACCCCCAA-3′). We performed PCR under the following conditions: an initial denaturation at 94 °C for 2 min followed by a cycle of denaturation at 94 °C for 1 min, annealing at 58 °C for 1 min and extension at 72 °C for 1 min. We subjected samples to 40 cycles followed by a final extension at 72 °C for 3 min. The products were analyzed on a 1.5% ethidium bromide stained agarose gel.

Immunocytochemistry. Cardiomyocytes or noncardiomyocytes of neonatal rats cultured on glass cover slips were incubated with or without the antibody to G-CSFR (Santa Cruz Biotechnology) for 1 h, followed by incubation with Cy3-labeled secondary antibodies. After washing, we double-stained the cells with fluorescent phalloidin (Molecular Probes) for 1 h at room temperature.

Western blots. Western blot analysis was performed as described[5]. We probed the membranes with antibodies to phospho-Jak2, phospho-Stat3 (Cell Signaling), phospho-Jak1, phospho-Tyk2, phospho-Stat1, phospho-Stat5, anti-Jak1, Jak2, Tyk2, Stat1, Stat3, Stat5, Bcl-2, Bax, G-CSFR (Santa Cruz Biotechnology), Bcl-xL, Bad (Transduction Laboratories) or actin (Sigma-Aldrich). We used the ECL system (Amersham Biosciences Corp) for detection.

Animals and surgical procedures. Generation and genotyping of dnStat3-Tg mice have been previously described[28]. All mice used in this study were 8–10-week-old males, unless indicated. All experimental procedures were performed according to the guidelines established by Chiba University for experiments in animals and all protocols were approved by our institutional review board. We anesthetized mice by intraperitoneally injecting a mixture of 100 mg/kg ketamine and 5 mg/kg xylazine. Myocardial infarction was produced by ligation of the left anterior descending artery. We operated on dnStat3-Tg mice to induce myocardial infarction and randomly divided them into two groups, the G-CSF-treated group (10–100 μg/kg/d subcutaneously for 5 d consecutively, Kyowa Hakko Kogyo Co.) and the saline-treated group. We operated on nontransgenic mice as control groups using the same procedures and divided them into a G-CSF-treated group and a saline-treated group. Some mice were randomly chosen to be analyzed for initial area at risk by injection of Evans blue dye after producing myocardial infarction. There was no difference in initial area sizes at risk between saline-treated control and G-CSF-treated mice ($n = 5$; **Supplementary Fig. 11** online). We also determined initial infarct size by triphenyltetrazolium chloride staining on day 3. There was no significant difference in initial infarct size between saline-treated control and G-CSF-treated mice ($n = 5$; **Supplementary Fig. 12** online).

Echocardiography and catheterization. Transthoracic echocardiography was performed with an Agilent Sonos 4500 (Agilent Technology Co.) provided with an 11-MHz imaging transducer. For catheterization analysis, the right carotid artery was cannulated under anesthesia by the micro pressure transducers with an outer diameter of 0.42 mm (Samba 3000; Samba Sensors AB), which was then advanced into the left ventricle. Pressure signals were recorded using a MacLab 3.6/s data acquisition system (AD Instruments) with a sampling rate of 2,000 Hz. Mice were anesthetized as described above, and heart rate was kept at approximately 270–300 beats per minute to minimize data deviation when we measured cardiac function.

Histology. Hearts fixed in 10% formalin were embedded in paraffin, sectioned at 4 μm thickness, and stained with Masson trichrome. The extent of fibrosis was measured in three sections from each heart and the value was expressed as the ratio of Masson trichrome stained area to total left ventricular free wall. For apoptosis analysis, infarcted hearts were frozen in cryomolds, sectioned, and TUNEL labeling was performed according to the manufacturer's protocol (*In Situ* Apoptosis Detection kit; Takara) in combination with immunostainings for appropriate cell markers. Digital photographs were taken at magnification ×400, and 25 random high-power fields (HPF) from each heart sample were chosen and quantified in a blinded manner. We examined vascularization by measuring the number of capillary endothelial cells in light-microscopic sections taken from the border zone of the hearts 2 weeks after myocardial infarction. Capillary endothelial cells were identified by immunohistochemical staining with antibody to platelet endothelial cell adhesion molecule (PECAM; Pharmingen). Ten random microscopic fields in the border zone were examined and the number of endothelial cells was expressed as the number of PECAM-positive cells/HPF (magnification, ×400).

Statistical analysis. Data are shown as mean ± s.e.m. Multiple group comparison was performed by one-way analysis of variance (ANOVA) followed by the Bonferroni procedure for comparison of means. Comparison between two groups were analyzed by the two-tailed Student's *t*-test or two-way ANOVA. Values of $P < 0.05$ were considered statistically significant.

URL. Alliance for Cellular Signaling Procedure Protocols
http://www.signaling-gateway.org/data/cgi-bin/Protocols.cgi?cat=0

Note: Supplementary information is available on the Nature Medicine website.

ACKNOWLEDGMENTS
The authors thank J. Robbins (Children's Hospital Research Foundation, Cincinnati, Ohio) for a fragment of the αMHC gene promoter, M. Tamagawa for the analysis of Langendorff-perfused model, Kirin Brewery Co., Ltd. for their kind gift of G-CSF, and M. Watanabe and E. Fujita for their technical assistance. This work was supported by a Grant-in-Aid for Scientific Research, Developmental Scientific Research, and Scientific Research on Priority Areas from the Ministry of Education, Science, Sports, and Culture and by the Program for Promotion of Fundamental Studies in Health Sciences of the Organization for Drug ADR Relief, R&D Promotion and Product Review of Japan (to I.K.) and Japan Research Foundation for Clinical Pharmacology (to T.M.).

COMPETING INTERESTS STATEMENTS
The authors declare that they have no competing financial interests.

Received 8 September 2004; accepted 19 January 2005
Published online at http://www.nature.com/naturemedicine/

1. Orlic, D. *et al.* Mobilized bone marrow cells repair the infarcted heart, improving function and survival. *Proc. Natl. Acad. Sci. USA* **98**, 10344–10349 (2001).
2. Ohtsuka, M. *et al.* Cytokine therapy prevents left ventricular remodeling and dysfunction after myocardial infarction through neovascularization. *FASEB J.* **18**, 851–853 (2004).
3. Moon, C. *et al.* Erythropoietin reduces myocardial infarction and left ventricular functional decline after coronary artery ligation in rats. *Proc. Natl. Acad. Sci. USA* **100**, 11612–11617 (2003).
4. Parsa, C.J. *et al.* A novel protective effect of erythropoietin in the infarcted heart. *J. Clin. Invest.* **112**, 999–1007 (2003).
5. Zou, Y. *et al.* Leukemia inhibitory factor enhances survival of cardiomyocytes and induces regeneration of myocardium after myocardial infarction. *Circulation* **108**, 748–753 (2003).
6. Minatoguchi, S. *et al.* Acceleration of the healing process and myocardial regeneration may be important as a mechanism of improvement of cardiac function and remodeling by postinfarction granulocyte colony-stimulating factor treatment. *Circulation* **109**, 2572–2580 (2004).
7. Adachi, Y. *et al.* G-CSF treatment increases side population cell infiltration after myocardial infarction in mice. *J. Mol. Cell. Cardiol.* **36**, 707–710 (2004).
8. Kawada, H. *et al.* Nonhematopoietic mesenchymal stem cells can be mobilized and differentiate into cardiomyocytes after myocardial infarction. *Blood* **104**, 3581–3587 (2004).
9. Avalos, B.R. Molecular analysis of the granulocyte colony-stimulating factor receptor. *Blood* **88**, 761–777 (1996).
10. Demetri, G.D. & Griffin, J.D. Granulocyte colony-stimulating factor and its receptor. *Blood* **78**, 2791–808 (1991).
11. Berliner, N. *et al.* Granulocyte colony-stimulating factor induction of normal human bone marrow progenitors results in neutrophil-specific gene expression. *Blood* **85**, 799–803 (1995).
12. Orlic, D. *et al.* Bone marrow cells regenerate infarcted myocardium. *Nature* **410**, 701–705 (2001).
13. Asahara, T. *et al.* Bone marrow origin of endothelial progenitor cells responsible for postnatal vasculogenesis in physiological and pathological neovascularization. *Circ. Res.* **85**, 221–228 (1999).
14. Kocher, A.A. *et al.* Neovascularization of ischemic myocardium by human bone-marrow-derived angioblasts prevents cardiomyocyte apoptosis, reduces remodeling and improves cardiac function. *Nat. Med.* **7**, 430–436 (2001).
15. Jackson, K.A. *et al.* Regeneration of ischemic cardiac muscle and vascular endothelium by adult stem cells. *J. Clin. Invest.* **107**, 1395–1402 (2001).
16. Balsam, L.B. *et al.* Haematopoietic stem cells adopt mature haematopoietic fates in ischaemic myocardium. *Nature* **428**, 668–673 (2004).
17. Murry, C.E. *et al.* Haematopoietic stem cells do not transdifferentiate into cardiac myocytes in myocardial infarcts. *Nature* **428**, 664–668 (2004).
18. Norol, F. *et al.* Influence of mobilized stem cells on myocardial infarct repair in a nonhuman primate model. *Blood* **102**, 4361–4368 (2003).
19. Aarts, L.H., Roovers, O., Ward, A.C. & Touw, I.P. Receptor activation and 2 distinct COOH-terminal motifs control G-CSF receptor distribution and internalization kinetics. *Blood* **103**, 571–579 (2004).
20. Benekli, M., Baer, M.R., Baumann, H. & Wetzler, M. Signal transducer and activator of transcription proteins in leukemias. *Blood* **101**, 2940–2954 (2003).
21. Smithgall, T.E. *et al.* Control of myeloid differentiation and survival by Stats. *Oncogene* **19**, 2612–2618 (2000).
22. Dumont, E.A. *et al.* Cardiomyocyte death induced by myocardial ischemia and reperfusion: measurement with recombinant human annexin-V in a mouse model. *Circulation* **102**, 1564–1568 (2000).
23. van Heerde, W.L. *et al.* Markers of apoptosis in cardiovascular tissues: focus on Annexin V. *Cardiovasc. Res.* **45**, 549–559 (2000).
24. Bromberg, J. Stat proteins and oncogenesis. *J. Clin. Invest.* **109**, 1139–1142 (2002).
25. El-Adawi, H. *et al.* The functional role of the JAK-STAT pathway in post-infarction remodeling. *Cardiovasc. Res.* **57**, 129–138 (2003).
26. Matsuura, K. *et al.* Adult cardiac Sca-1-positive cells differentiate into beating cardiomyocytes. *J. Biol. Chem.* **279**, 11384–11391 (2004).
27. Zou, Y. *et al.* Both Gs and Gi proteins are critically involved in isoproterenol-induced cardiomyocyte hypertrophy. *J. Biol. Chem.* **274**, 9760–9770 (1999).
28. Funamoto, M. *et al.* Signal transducer and activator of transcription 3 is required for glycoprotein 130-mediated induction of vascular endothelial growth factor in cardiac myocytes. *J. Biol. Chem.* **275**, 10561–10566 (2000).
29. Ikeda, K. *et al.* The effects of sarpogrelate on cardiomyocyte hypertrophy. *Life Sci.* **67**, 2991–2996 (2000).

ELSEVIER

CYTOKINE

www.elsevier.com/locate/issn/10434666

Cytokine 28 (2004) 186–189

Reciprocal regulation of permeability through a cultured keratinocyte sheet by IFN-γ and IL-4

Junichi Kobayashi[a,b,*], Tetsuichiro Inai[a], Keisuke Morita[b], Yoichi Moroi[b], Kazunori Urabe[b], Yosaburo Shibata[a], Masutaka Furue[b]

[a]*Department of Developmental Molecular Anatomy, Graduate School of Medical Sciences, Kyushu University, Fukuoka 812-8582, Japan*
[b]*Department of Dermatology, Graduate School of Medical Sciences, Kyushu University, Fukuoka 812-8582, Japan*

Received 24 November 2003; received in revised form 19 May 2004; accepted 2 August 2004

Abstract

The T cell cytokines profoundly modify the phenotypic and functional characteristics of keratinocytes. Until now, no study has focused on the effect of Th1 and Th2 cytokines on keratinocyte permeability. Using a two-layer well culturing system, permeability was assessed through cultured keratinocyte sheet in the presence or absence of various concentrations of IFN-γ and IL-4. Transepithelial electrical resistance (TER) and the flux of 40 kDa FITC-dextrans were measured across the cultured keratinocyte sheet. IFN-γ significantly increased the TER in a dose- and time-dependent manner, suggesting that IFN-γ profoundly inhibited the permeability of ions through the keratinocyte sheet. In contrast, IL-4 did not affect the TER. When compared to medium control, the flux of FITC-dextran of the IFN-γ group was significantly decreased in a dose-dependent fashion. In sharp contrast, the flux of FITC-dextran was significantly and dose-dependently increased in the presence of IL-4. A significant increase in TER and a significant decrease in the flux of dextran suggested that IFN-γ clearly reduced the permeability of both ions and high molecular weight material through the keratinocyte sheet. Although IL-4 did not affect the permeability of the ions, it significantly enhanced the permeability of high molecular weight material. A flow cytometric assay revealed that the expression of desmoglein-3 was suppressed by IL-4, but was enhanced by IFN-γ. The reciprocal regulation of permeability of the cultured keratinocyte sheet by IFN-γ and IL-4 may be partly related to the modification of intercellular adhesion molecules.

Keywords: Keratinocyte; Permeability; IFN-γ; IL-4

1. Introduction

Epidermis, a squamous epithelium of the skin, serves as the outermost barrier of the body, separating it from the surrounding environment and preventing the loss of body fluids and proteins. Very frequently, immunological and inflammatory processes result in skin damage in eczematous disorders such as contact dermatitis and atopic dermatitis [1,2]. Eczema is an orchestrated cellular response conducted by various immunocompetent cells, including Th1 and the Th2 cells, that produce large amounts of cytokines such as IFN-γ and IL-4, respectively [3,4]. One of the characteristic manifestations of eczema is serous papules with spongiosis and oozing, which may result from an increased permeability of body fluids into the epidermal compartment.

Previous studies have shown that T cell cytokines profoundly modify the phenotypic and functional characteristics of keratinocytes [5,6]. However, there have been no reports investigating the effect of Th1 and

* Corresponding author. Division of Dermatology, Nippon Steel Yawata Memorial Hospital, 1-1-1, Harunomachi, Yahatahigashi-ku, Kitakyushu J-805-8508, Japan. Tel.: +81 93 672 3176; fax: +81 93 671 9605.
E-mail address: jkobayashi@jcom.home.ne.jp (J. Kobayashi).

1043-4666/$ - see front matter © 2004 Elsevier Ltd. All rights reserved.
doi:10.1016/j.cyto.2004.08.003

Th2 cytokines on the permeability of keratinocytes. We recently demonstrated that IL-4 down-regulated the cell surface expression of an adhesion molecule, E-cadherin, whereas IFN-γ up-regulated its expression [7]. This finding suggested that IL-4 and IFN-γ may modify the permeability of keratinocyte. In the present study, we examined the effects of IFN-γ and IL-4 on the trans-epithelial electrical resistance (TER) and the flux of 40 kDa FITC-dextrans across a cultured keratinocyte sheet.

2. Results

2.1. IFN-γ increased the TER of the keratinocyte sheet

We first examined the effects of IFN-γ and IL-4 on the TER of the keratinocyte sheet. The TER values represent the permeability of water-soluble ions. IFN-γ significantly increased the electrical resistance in a dose- and time-dependent manner (Fig. 1). In particular, the values of TER after treating the cultured sheet with 2 ng/ml of IFN-γ were approximately three times higher than those of the medium control, suggesting that IFN-γ profoundly inhibited the permeability of ions through the keratinocyte sheet. In contrast, IL-4 did not affect the TER (Fig. 1).

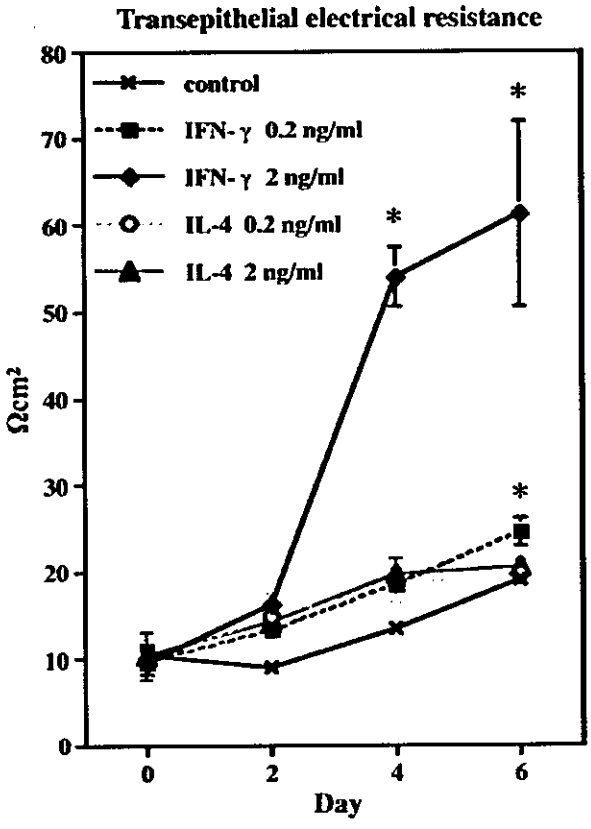

Fig. 1. The TER was measured across the confluent HaCaT keratinocyte sheet every second day using a Millicell-ERS epithelial voltohmmeter. IFN-γ significantly increased the TER in a dose- and time-dependent manner. In contrast, IL-4 did not affect the TER. The values indicated are means ± SD ($n = 4$). *$p < 0.01$ compared with the control.

2.2. Down-regulation of the flux of FITC-dextran through the keratinocyte sheet by IFN-γ and its up-regulation by IL-4

Next, we examined whether IFN-γ or IL-4 may modify the permeability of high molecular weight material through the keratinocyte sheet using 40 kDa FITC-dextran. As shown in Fig. 2, IFN-γ significantly decreased the flux of FITC-dextran in a dose-dependent fashion compared to the medium control (81.3% inhibition at 2 ng/ml of IFN-γ). In sharp contrast, IL-4 dose-dependently up-regulated the flux of FITC-dextran (92.3% up-regulation at 2 ng/ml of IL-4).

2.3. Desmoglein-3 expression was up-regulated by IFN-γ, but was down-regulated by IL-4

Desmoglein-3 is one of the major intercellular adhesion molecules between keratinocytes. Therefore, we investigated whether the expression of desmoglein-3 is modulated by IL-4 or IFN-γ. The expression of desmoglein-3 was dramatically up-regulated by IFN-γ and was down-regulated by IL-4 (Fig. 3).

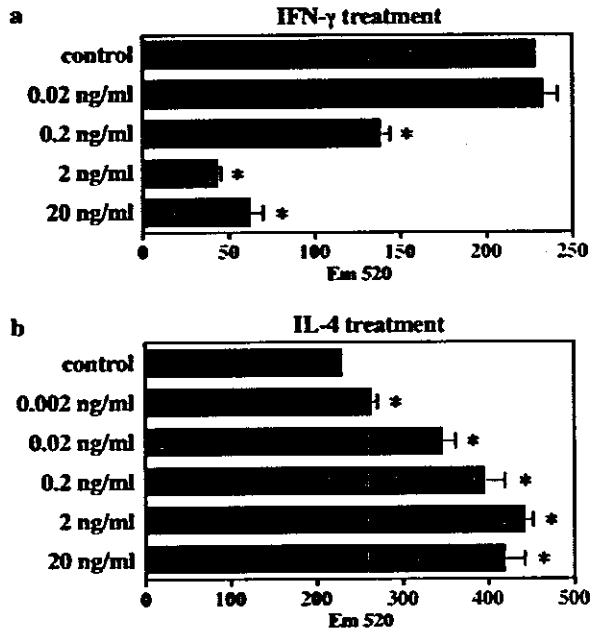

Fig. 2. The flux of 40 kDa FITC-dextrans was measured using a fluorometer (excitation, 492 nm; emission, 520 nm). IFN-γ dose-dependently inhibited the permeability of FITC-dextran, whereas IL-4 enhanced its permeability. The values indicated are means ± SD ($n = 4$). *$p < 0.01$ compared to the control.

3. Discussion

TER and the flux assay have been demonstrated to be a suitable in vitro models to determine the permeability of water-soluble ions and solutes containing various molecular weight materials, respectively [8,9]. FITC-labeled dextrans with a molecular weight of 40 kDa, which are similar in molecular weight to plasma albumin, were utilized in the flux assay as a tracer. In this study, we demonstrated a significant increase in TER and a significant decrease in the flux of dextran by IFN-γ, suggesting that IFN-γ may reduce the permeability of both ions and high molecular weight material through the keratinocyte sheet. In contrast, IL-4 significantly enhanced the permeability of dextran. We did not detect an effect of IL-4 on the TER of the keratinocyte sheet. Interestingly, Ahdieh et al. recently investigated the permeability of cultured lung epithelial cells and found that IL-4 treatment resulted in a 70–75% increase in permeability, as assessed by electrophysiological and mannitol flux measurements. In contrast, IFN-γ markedly reduced the permeability [10]. However, the means that IFN-γ and IL-4 modify the permeability are unknown.

Ye et al. have reported that the expression of IL-1 and its receptor plays a pivotal role in permeability homeostasis in the epidermis [2]. IFN-γ and IL-4 may alter the IL-1/IL-1 receptor signaling system. In fact, IFN-γ augments IL-1 production [11]. The expression of adhesion molecules may be related to the permeability of keratinocytes. Trautmann et al. demonstrated a reduced expression of E-cadherin in areas of spongiosis in acute eczematous dermatitis. They also showed that the induction of keratinocyte apoptosis is accompanied by a rapid cleavage of E-cadherin [12]. Recently, we found that IL-4 down-regulated the cell surface expression of E-cadherin, whereas IFN-γ up-regulated its expression [7]. In the present study, we showed that the expression of desmoglein-3 was also enhanced by IFN-γ but was inhibited by IL-4. The modification of these intercellular adhesion molecules occurred earlier than the permeability change and required higher concentrations of cytokines, however, it may be partly responsible for the permeability of keratinocytes.

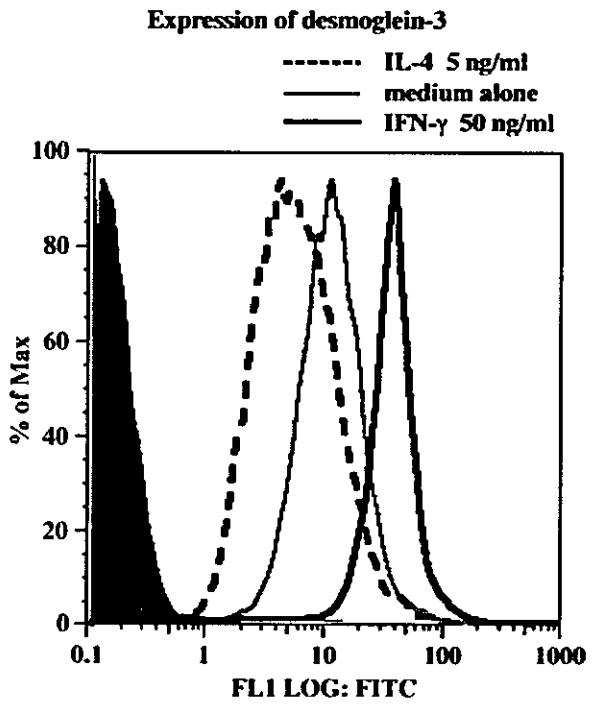

Fig. 3. Keratinocytes were cultured with IFN-γ (50 ng/ml), IL-4 (5 ng/ml) or medium alone for 48 h and the expression of desmoglein-3 was analyzed by flow cytometry. IFN-γ augmented the expression of desmoglein-3, while IL-4 decreased its expression.

4. Material and methods

4.1. Cell culture

HaCaT keratinocytes (a kind gift from Dr. N.E. Fusening in Heidelberg) were maintained in Dulbecco's modified Eagle medium (DMEM) supplemented with 10% fetal bovine serum (FBS), 100 IU/ml penicillin, and 100 μg/ml streptomycin (GIBCO BRL, Rockville, MD/USA). Using a two-layer well culturing system, cells were plated at a confluent density, at about 3×10^5 cells/cm^2, on 12-mm membrane culture inserts (0.6 cm^2; Millipore Corp., Bedford, MA/USA) in a 24-well plate. After an overnight incubation for cell attachment, we added various concentrations of IFN-γ (0.02–20 ng /ml) or IL-4 (0.002–20 ng/ml) into the outer layer culture medium, and further cultured the cells for up to 6 days. Assays for the permeability of keratinocyte sheets were performed as described below.

4.2. Measurement of the TER

The TER was measured using a Millicell-ERS epithelial voltohmmeter (Millipore), as described previously [13]. The TER values were calculated by subtracting the contribution of the bare filter and medium and multiplying by the surface area of the filter. The TER represents the transepithelial permeability of the water-soluble ions. A higher value of TER means a lower permeability of ions. These data were analyzed using the Student's t test. A p value of less than 0.01 was considered to be statistically significant. The experiment was repeated at least three times in quadruplicate.

4.3. Measurement of flux of FITC-dextran

The cells were cultured at confluence with or without various concentrations of IFN-γ or IL-4 for 6 days on culture insert. The flux was measured as described previously [13]. In brief, the culture medium was replaced with P buffer (10 mM Hepes, pH 7.4, 1 mM sodium pyruvate, 10 mM glucose, 3 mM $CaCl_2$, 145 mM NaCl), and 1 mg/ml FITC-dextran (40 kDa: Sigma, St. Louis, MO/USA) was added to the outer wells. At 120 min after the addition of FITC-dextran into the outer chambers, the media from the inner wells were collected, and the flux of FITC-dextran was measured with a fluorometer RF-1500 (Shimadzu, Tokyo, Japan). The flux of FITC-dextran represents the permeability of the solutes with high molecular weight material beyond the keratinocyte sheet. These data were analyzed using the Student's t test. A p value of less than 0.01 was considered to be statistically significant. The experiment was repeated at least three times in quadruplicate.

4.4. Flow cytometry

The HaCaT keratinocytes were cultured in the presence or absence of IL-4 (5 ng/ml) or IFN-γ 50 ng/ml) for 48 h. Cells were detached from the plates using trypsine–EDTA and were incubated with mouse anti-desmoglein-3 antibody (Zymed, San Francisco, California, USA) or isotype-matched control antibody (Zymed) for 30 min on ice. After washing, the cells were incubated with FITC-conjugated goat anti-mouse IgG antibody (Molecular Probes, Eugene, OR). The stained cells were analyzed by flow cytometry (EPIX-XL, Coulter, Fullerton, CA).

Acknowledgements

This work was supported in part by grants from Koga Hideya Funds and Grants-in-Aid for Scientific Research from the Ministry of Education, Science and Culture, Japan (Nos. 08770015, 09770010 and 11770008).

References

[1] Gfesser M, Rakoski J, Ring J. The disturbance of epidermal barrier function in atopy patch test reactions in atopic eczema. Br J Dermatol 1996;135:560–5.
[2] Ye J, Garg A, Calhoun C, Feingold KR, Elias PM, Ghadially R. Alterations in cytokine regulation in aged epidermis: implications for permeability barrier homeostasis and inflammation. I. IL-1 gene family. Exp Dermatol 2002;11:209–16.
[3] Hamid Q, Boguniewicz M, Leung DY. Differential in situ cytokine gene expression in acute versus chronic atopic dermatitis. J Clin Invest 1994;94:870–6.
[4] Tamaki K, Nakamura K. The role of lymphocytes in healthy and eczematous skin. Curr Opin Allergy Clin Immunol 2001;1: 455–60.
[5] Uchi H, Terao H, Koga T, Furue M. Cytokines and chemokines in the epidermis. J Dermatol Sci 2000;24(1):S29–38.
[6] Vestergaard C, Kirstejn N, Gesser B, Mortensen JT, Matsushima K, Larsen CG. IL-10 augments the IFN-γ and TNF-α induced TARC production in HaCaT cells: a possible mechanism in the inflammatory reaction of atopic dermatitis. J Dermatol Sci 2001;26:46–54.
[7] Fujii-Maeda S, Kajiwara K, Ikizawa K, Shinazawa M, Yu B, Koga T, et al. Reciprocal regulation of TARC/MDC production by IL-4/IL-13 and IFN-γ in HaCaT keratinocytes is mediated by alternations in E-cadherin distribution. J Invest Dermatol 2004; 122:20–8.
[8] Mullin JM, Marano CW, Laughlin KV, Nuciglio M, Stevenson BR, Soler P. Different size limitations for increased transepithelial paracellular solute flux across phorbol ester and tumor necrosis factor-treated epithelial cell sheets. J Cell Physiol 1997;171:226–33.
[9] Francis SA, Kelly JM, McCormack J, Rogers RA, Lai J, Schneeberger EE, et al. Rapid reduction of MDCK cell cholesterol by methyl-beta-cyclodextrin alters steady state transepithelial electrical resistance. Eur J Cell Biol 1999;78:473–84.
[10] Ahdieh M, Vandenbos T, Youakim A. Lung epithelial barrier function and wound healing are decreased by IL-4 and IL-13 and enhanced by IFN-γ. Am J Physiol Cell Physiol 2001;281: C2029–38.
[11] Wei L, Debets R, Hegmans JJ, Benner R, Prens EP. IL-1 β and IFN-γ induce the regenerative epidermal phenotype of psoriasis in the transwell skin organ culture system. IFN-γ up-regulates the expression of keratin 17 and keratinocyte transglutaminase via endogenous IL-1 production. J Pathol 1999;187:358–64.
[12] Trautmann A, Altznauer F, Akdis M, Simon HU, Disch R, Brocker EB, et al. The differential fate of cadherins during T-cell-induced keratinocyte apoptosis leads to spongiosis in eczematous dermatitis. J Invest Dermatol 2001;117:927–34.
[13] Inai T, Kobayashi J, Shibata Y. Claudin-1 contributes to the epithelial barrier function in MDCK cells. Eur J Cell Biol 1999;78: 849–55.

THE JOURNAL OF BIOLOGICAL CHEMISTRY
Vol. 279, No. 48, Issue of November 26, pp. 50537–50554, 2004
Printed in U.S.A.

Vascular Endothelial Growth Factor- and Thrombin-induced Termination Factor, Down Syndrome Critical Region-1, Attenuates Endothelial Cell Proliferation and Angiogenesis*[S]♦

Received for publication, June 10, 2004, and in revised form, September 17, 2004
Published, JBC Papers in Press, September 23, 2004, DOI 10.1074/jbc.M406454200

Takashi Minami‡§, Keiko Horiuchi‡, Mai Miura‡, Md. Ruhul Abid¶, Wakako Takabe‡, Noriko Noguchi‡, Takahide Kohro‡, Xijin Ge‡, Hiroyuki Aburatani‡, Takao Hamakubo‡, Tatsuhiko Kodama‡§, and William C. Aird¶‖

From the ‡The Research Center for Advanced Science and Technology, the University of Tokyo, Tokyo 153-8904, Japan and ¶The Department of Molecular and Vascular Medicine, Beth Israel Deaconess Medical Center/Harvard Medical School, Boston, Massachusetts 02215

Activation and dysfunction of the endothelium underlie many vascular disorders including atherosclerosis, tumor growth, and inflammation. Endothelial cell activation is mediated by many different extra-cellular signals, which result in overlapping yet distinct patterns of gene expression. Here we show, in DNA microarray analyses, that vascular endothelial growth factor (VEGF) and thrombin result in dramatic and rapid up-regulation of Down syndrome critical region (DSCR)-1 gene encoding exons 4–7, a negative feedback regulator of calcium-calcineurin-NF-AT signaling. VEGF- and thrombin-mediated induction of DSCR-1 involves the cooperative binding of NF-ATc and GATA-2/3 to neighboring consensus motifs in the upstream promoter. Constitutive expression of DSCR-1 in endothelial cells markedly impaired NF-ATc nuclear localization, proliferation, and tube formation. Under *in vivo* conditions, overexpression of DSCR-1 reduced vascular density in matrigel plugs and melanoma tumor growth in mice. Taken together, these findings support a model in which VEGF- and thrombin-mediated induction of endothelial cell proliferation triggers a negative feedback loop consisting of DSCR-1 gene induction and secondary inhibition of NF-AT signaling. As a natural brake in the angiogenic process, this negative pathway may lend itself to therapeutic manipulation in pathological states.

The endothelium is highly malleable cell layer, constantly responding to changes within the extracellular environment and responding in ways that are usually beneficial, but at times harmful, to the organism. Several mediators, including growth factors (*e.g.* vascular endothelial growth factor (VEGF)[1]), cytokines (*e.g.* tumor necrosis factor-α (TNF-α)), and serine proteases (*e.g.* thrombin), activate gene transcription in endothelial cells, resulting in changes in hemostatic balance, increased leukocyte adhesion, loss of barrier function, increased permeability, migration, proliferation, and successive angiogenesis. The tight control of these processes is essential for homeostasis; endothelial cell activation, if excessive, sustained, or spatially and temporally misplaced, may result in vasculopathic disease. Under normal conditions, the activation signal may be terminated by negative feedback inhibition of downstream transcriptional networks. Such a mechanism has been well established for TNF-α (1–4). In contrast, little is known about the major self-regulatory processes involved in VEGF and thrombin signaling.

VEGF is an endothelial cell-specific mitogen, and chemotactic agent, which is involved in wound repair, angiogenesis of ischemic tissue, tumor growth, microvascular permeability, hemostasis, and endothelial cell survival (5, 6). VEGF binds to two receptor-type tyrosine kinases, Flt-1 and Flk-1/KDR (7, 8). A third receptor, neuropilin, has been identified, but its role in VEGF signaling has not been fully elucidated (9). The VEGF receptors have been shown to activate a number of different intracellular signaling pathways, including PKC (10), PI3K and Akt/PKB (11), MEK1/2 (12), p38 MAPK (13), and phospholipase C (14).

Thrombin is a multifunctional serine protease that is involved not only in mediating the cleavage of fibrinogen to fibrin in the coagulation cascade but also in activating a variety of cell types, including platelets and endothelial cells. Thrombin signaling in the endothelium may result in a multitude of phenotypic changes, including alterations in cell shape, permeability, vasomotor tone, leukocyte trafficking, migration, DNA synthesis, angiogenesis, and hemostasis (15). Thrombin signaling in the endothelium is mediated by a family of seven-transmembrane G-protein-coupled receptors, termed protease activated receptors (PAR) (16). Currently, four members of the PAR family have been identified (PAR-1 to PAR-4). Of the various PAR family members, PAR-1 is the predominant thrombin receptor in endothelial cells (17). Once activated, PAR-1 is linked to a number of signal intermediates that include, but are not limited to, MAPK, protein kinase C, PI3K, and Akt (15, 18).

* This work was supported in part by grants-in-aid from the Ministry of Education, Science, Sports and Culture of Japan (to T. M.) and by the Uehara Memorial Foundation in Japan (to T. M.). The costs of publication of this article were defrayed in part by the payment of page charges. This article must therefore be hereby marked "*advertisement*" in accordance with 18 U.S.C. Section 1734 solely to indicate this fact.

♦ This article was selected as a Paper of the Week.

[S] The on-line version of this article (available at http://www.jbc.org) contains supplemental Fig. 1 and Tables I and II.

§ To whom all corresponding may be addressed: The Research Center for Advanced Science and Technology, the University of Tokyo, 4-6-1 Komaba, Meguro, Tokyo 153-8904, Japan. Tel.: 81-3-5452-5403; Fax: 81-3-5452-5232; E-mail: minami@med.rcast.u-tokyo.ac.jp (for T. M.) and kodama@lsbm.org (for T. K.).

‖ Supported in part by National Institutes of Health Grant HL36028.

[1] The abbreviations used are: VEGF, vascular endothelial growth factor; TNF-α, tumor necrosis factor-α; PAR, protease activated receptor; MAPK, mitogen-activated protein kinase; PI3K, phosphatidylinositol 3-kinase; HUVEC, human umbilical vein endothelial cells; TRAP, thrombin receptor activation peptide; PlGF, placenta growth factor; EGM, endothelial growth medium; Ad, adenovirus; EMSA, electrophoretic mobility shift assay; FACS, fluorescence-activated cell sorter; PBS, phosphate-buffered saline; CsA, cyclosporine A; EGFP, enhanced green fluorescent protein; GAPDH, glyceraldehyde-3-phosphate dehydrogenase; RT, reverse transcription; IRES, internal ribosome entry.

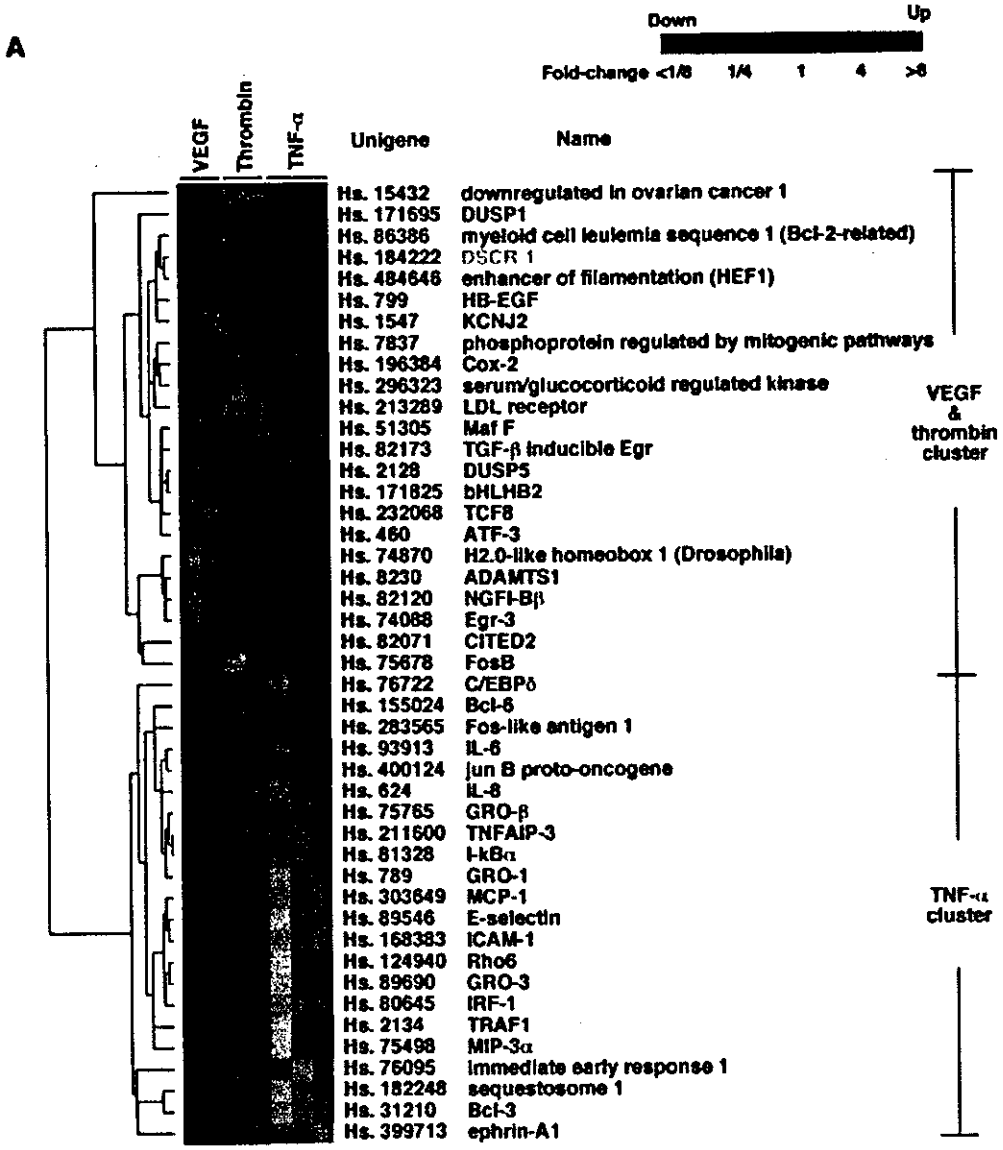

B

the five highest induced genes at 1 h

VEGF-mediated genes	1 DSCR-1 22.3-fold	2 Egr-3 17.0-fold	3 NGFI-Bβ 11.9-fold	4 COX-2 8.1-fold	5 ADAMTS1 7.2-fold
thrombin-mediated genes	1 DSCR 1 17.7-fold	2 FosB 17.5-fold	3 IL-8 10.7-fold	4 COX-2 10.4-fold	5 GRO-β 10.1-fold
TNF-α-mediated genes	1 E-selectin 87.1-fold	2 GRO-β 54.1-fold	3 GRO-1 35.7-fold	4 ICAM-1 24.3-fold	5 GRO-3 22.4-fold

FIG. 1. **DSCR-1 is the most highly induced early response gene in VEGF- and thrombin-treated HUVEC.** *A*, cluster analysis of early response genes (1 h). *B*, the average fold induction of the five most highly induced genes in VEGF-, thrombin-, and TNF-α-treated HUVEC.

Given the overlapping functions of VEGF and thrombin both in terms of signaling pathways activated and phenotypic response, we hypothesized that these two mediators are likely to trigger common transcriptional networks in the endothelium. To identify such factors, we compared DNA microarray analyses of VEGF and thrombin-treated human umbilical vein endothelial cells (HUVEC). We found that under both conditions, the most highly induced gene was DSCR-1. The DSCR-1 gene (also known as MCIP-1), designated as such because it resides within the Down syndrome critical region of human chromosome 21, encodes a protein that binds to and inhibits the catalytic subunit of calcineurin (19). In this report, we show that DSCR-1 acts as a "circuit breaker" in VEGF and thrombin signaling, serving in a negative feedback loop to inhibit endothelial cell proliferation and activation as well as angiogenesis. These results provide new insights into endothelial cell signaling and point to DSCR-1 as a potential therapeutic target for anti-angiogenesis and anti-inflammatory therapy.

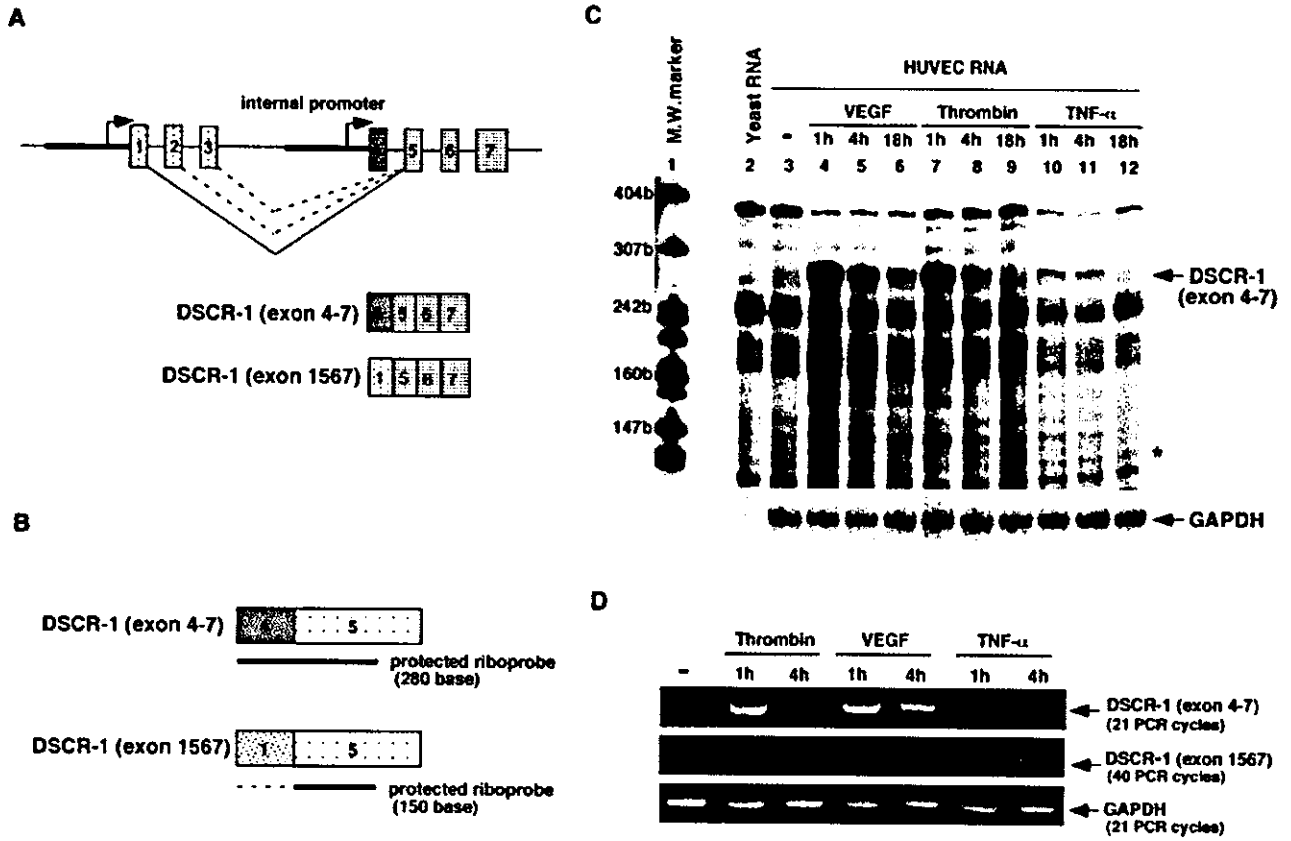

FIG. 2. **DSCR-1 isoform consisting of exons 4–7 was selectively induced with VEGF and thrombin treatments in primary human endothelial cells.** *A*, schematic representation of the human DSCR-1 gene. The mRNA consists of four alternative first exons (*boxes 1–4*) followed by three common exons (*boxes 5–7*). The *broken line* indicates the putative splicing isoforms. Shown are the two major DSCR-1 isoforms, DSCR-1 (exon 4–7) and DSCR-1 (exon 1567). *B*, schematic representation of the riboprobe used to distinguish the two DSCR-1 isoforms in RNase protection assays. The *bold line* indicates the protected fragment and the *broken line* the RNase-digested region. *C*, RNase protection assays were performed with [α-^{32}P]UTP-labeled 361-bp riboprobe as shown in *B* and either 10 μg of yeast RNA (*lane 2*), 10 μg of total RNA from control (*lane 3*), VEGF-treated (*lanes 4–6*), thrombin-treated (*lanes 7–9*), or TNF-α-treated (*lanes 10–12*) HUVEC. The *arrow* indicates the protected fragment (280 bp) from the DSCR-1 (exon 4–7) isoform; the *asterisk* indicates the expected length (130 bp) from the DSCR-1 (exon 1567) isoform. An [α-^{32}P]UTP-labeled human GAPDH riboprobe was hybridized with total RNA as an internal control. *D*, RT-PCR was performed with either DSCR-1 (exons 4–7) or DSCR-1 (exon 1567) isoform-specific primers, using RNA from control (−) and thrombin-, VEGF-, or TNF-α-treated HUVEC and 21- or 40-cycle amplification. GAPDH-specific primers were included as an internal control.

EXPERIMENTAL PROCEDURES

Materials and Cell Culture—VEGF and TNF-α were obtained from Peprotec (Rocky Hill, NJ). Human thrombin, cyclosporine A, and SU1498 were obtained from Calbiochem. Hirudin and thrombin receptor activation peptide (TRAP; SFLLRNPNDKYEPF) were from Wako chemicals (Osaka, Japan). Human placenta growth factorPlGF) was from R&D Systems (Minneapolis, MN). HUVEC were grown in endothelial growth medium-2-MV (EGM-2-MV) BulletKit (Clonetics, San Diego, CA). HUVEC were used within the first eight passages. Mouse B16-melanoma cells (JCRB-0202) were grown in Dulbecco's modified Eagle's medium plus 10% fetal bovine serum.

Microarray Analysis—HUVEC were serum-starved overnight in medium containing EGM-2 and 0.5% fetal bovine serum and then treated with 50 ng/ml VEGF or 1.5 units/ml thrombin. RNA was harvested and purified with Trizol according to manufacturer's protocol (Invitrogen). Preparation of cRNA and hybridization of probe arrays were performed according to the protocols of the manufacturer (Affimetrix, Santa Clara, CA).

RNase Protection Assays and Reverse Transcription-PCR (RT-PCR)—HUVEC were serum-starved in EBM-2 medium containing 0.5% fetal bovine serum. 18 h later, HUVEC were pretreated for 30 min with cyclosporin A or SU1498 at the doses indicated or infected with adenovirus at multiplicity of infection = 40 and then incubated in the absence or presence of either 50 ng/ml VEGF, 1.5 units/ml thrombin, 10 ng/ml TNF-α, or 50–200 ng/ml PlGF. RNase protection assays were performed with a RPA III kit (Ambion) according to the manufacturer's instructions. For RT-PCR, a Superscript First-strand synthesis kit (Invitrogen) was used with 5 μg of total RNA. Forward and reverse primers and amplification cycles as follows: Tissue factor (22 cycles), 5′-TCAGAGTTTTGAACAGGTGGGAACA-3′ (forward) and 5′-TTCTCCTGGCCCATACACTCTACCG-3′ (reverse); E-selectin (22 cycles), 5′-CATGTGGAGCCACAGGACACTGGTCTG-3′ (forward) and 5′-TCTGATTCAAGGCTTTGGCAGCTGCTG-3′ (reverse); angiopoietin-2 (20 cycles), 5′-ACAAATGTATTTGCAAATGTTCACAAA-3′ (forward) and 5′-GAAATCTGCTGGTCGGATCATCATGGT-3′ (reverse); PlGF (20 cycles), 5′-CCGGTCATGAGGCTGTTCCCTTGC-3′ (forward) and 5′-CTCGCTGGGGTACTCGGACACGAC-3′ (reverse); P27 (26 cycles), 5′-CGCAGGAATAAGGAAGCGACCTGC-3′ (forward) and 5′-CGTTTGACGTCTTCTGAGGCCAGGCTT-3′ (reverse); P21 (18 cycles), 5′-AGCAAGGCCTGCCGCCGCCTCTTC-3′ (forward) and 5′-TGACAGGTCCACATGGTCTTCCTC-3′ (reverse); ADAMTS1 (20 cycles), 5′-AGCTTTCTTGCCATCAAAGCTGCT-3′ (forward) and 5′-A ACCTGGATGGTCAAGGGCTCTTT-3′ (reverse); interleukin-8 (23 cycles), 5′-TGTCAGTGCATAAAGACATACTCCA-3′ (forward) and 5′-CTTCTCCACAACCCTCTGCACCCAG-3′ (reverse); ICAM-1 (23 cycles), 5′-GTGCAAGAAGATAGCCAACCAATG-3′ (forward) and 5′-AGGAGTCGTTGCCATAGGTGACTG-3′ (reverse); cyclophilin A (23 cycles), 5′-TTCGTGCTCTGAGCACTGGAGA-3′ (forward) and 5′-GGACCCGTATGCTTTAGGATGAAG-3′ (reverse).

Transfections and Analysis of Luciferase Activity—HUVEC were transfected using FuGENE 6 reagent (Roche Applied Science) as described previously (20). The serum-starved transfected cells were preincubated for 30 min with 1 μM cyclosporine A and then incubated with 50 ng/ml VEGF or 1.5 units/ml thrombin for 6 h.

Electrophoretic Mobility Shift Assays (EMSAs)—Nuclear extracts purification and EMSAs were prepared as described previously (21). To test the effect of antibodies on DNA-protein binding, nuclear extracts were preincubated with antibodies of NF-ATc, NF-ATp (Affinity Bio-Reagents, Golden, CO), GATA-2, -3, or -6 (Perseus Proteomics, Tokyo, Japan) for 30 min at room temperature.

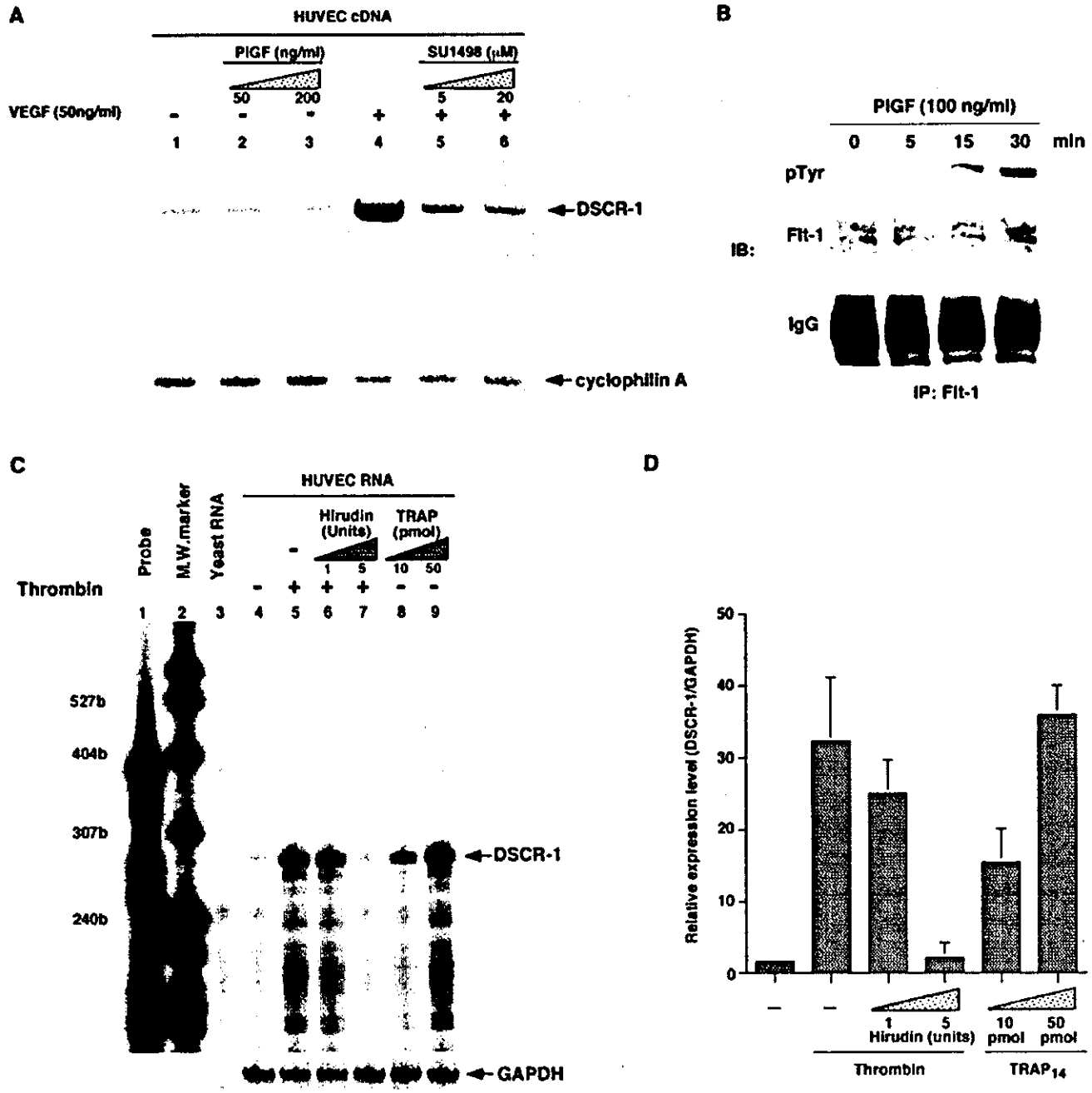

FIG. 3. **VEGF-Flk-1/KDR- and thrombin-PAR1-mediated up-regulation of DSCR-1 mRNA.** *A*, RT-PCR of DSCR-1 in HUVEC treated with 50 ng/ml PlGF (*lane 2*), 200 ng/ml PlGF (*lane 3*), pretreated with 5 μM SU1498 (*lane 5*), 20 μM SU1498 (*lane 6*), and treated in the absence (−) or presence (+) of 50 ng/ml VEGF for 1 h. Cyclophilin A-specific primers were added as an internal control. *B*, immunoprecipitation assays were performed in HUVEC treated with 100 ng/ml PlGF for 0, 5, 15, and 30 min. Total HUVEC lysates were subjected to immunoprecipitation (*IP*) using anti-Flt-1 antibody, then immunoblotted (*IB*) with anti-phosphotyrosine antiboby (*pTyr*). The same blots were stripped and reprobed with anti-Flt-1 antibody (*Flt-1*). IgG is shown as a loading control. *C*, RNase protection assays were performed with either no RNA (*lane 1*, *Probe*), 10 μg of yeast RNA (*lane 3*), or 10 μg of total RNA from control HUVEC (*lane 4*), thrombin-treated HUVEC pretreated in the absence (*lane 5*) or presence of 0.5 and 5 units of hirudin (*lanes 6* and *7*, respectively) or HUVEC treated with 10 or 50 pmol of TRAP (*lanes 8* and *9*, respectively). Human GAPDH was used as an internal control. *D*, quantification of RNase protection assays. Densitometry was used to calculate the ratio of DSCR-1 and GAPDH signals (arbitrary relative expression level). Mean and S.D. values were derived from three independent experiments.

FACS Analysis—Ad-DSCR-1-, Ad-Control-, or Ad-DSCR-1 plus Ad-CA-NFAT-infected HUVEC were scraped, spun down for 5 min at 100 × *g*, re-suspended in PBS containing with 0.2% Triton X, and stained in 25 μg/ml propidium iodide and 50 ng/ml RNase A. Cells were counted on a FACS Calibur using CellQuest software (BD Biosciences), and the percentages of cells in the G_1, S, and G_2/M phases of the cell cycle were determined using ModFit LT software (Verity Software House, Topsham, ME).

Immunolocalization Studies—HUVEC were plated onto glass coverslips (Matsunami Glass, Osaka, Japan) in a 6-well plate at a density of 25,000 cells/slide. The cells were treated in the presence or absence of 1 unit/ml thrombin or 50 ng/ml VEGF for 1 h, fixed in ice-cold 3.7% paraformaldehyde for 10 min, washed with PBS, and subsequently incubated with primary anti-NF-ATc antibody (Affinity BioReagents). Following extensive washes in PBS, the cells were incubated with an Alexa-Fluor 594-labeled secondary antibody (Molecular Probes, Eugene, OR) for 1 h. The slides were then washed in PBS, mounted in Crystal/Mount (Biomeda, Foster City, CA) with Hoechst (Sigma) for identification of nuclear localization, and examined by fluorescence microscopy. The degree of nuclear localization was quantified with NIH image.

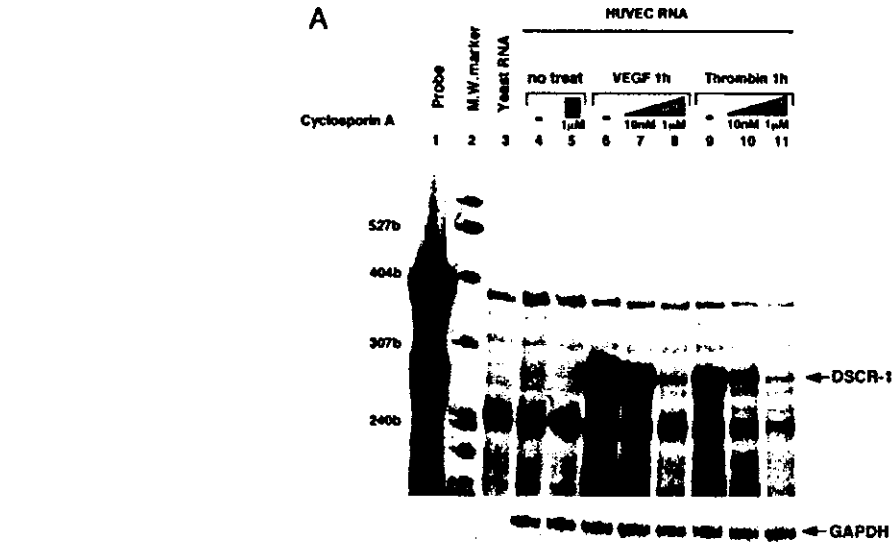

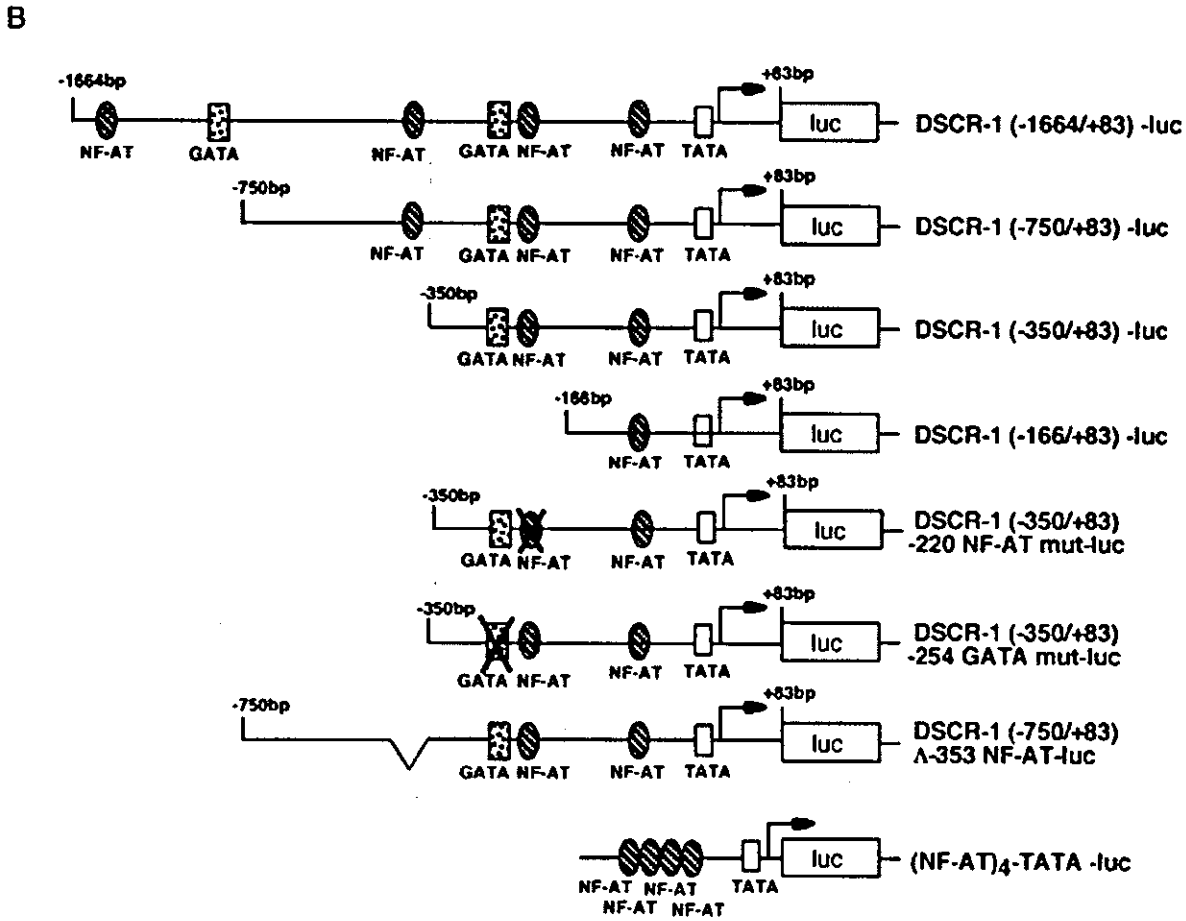

FIG. 4. **The NF-AT and GATA motif is necessary for mediating VEGF and thrombin stimulation of DSCR-1 mRNA and promoter in endothelial cells.** *A*, RNase protection assays were employed with either no RNA (*lane 1, Probe*), 10 μg of yeast RNA (*lane 3*), or 10 μg of total RNA from untreated HUVEC (*lanes 4* and *5*), VEGF-treated HUVEC (*lanes 6–8*), or thrombin-treated HUVEC (*lanes 9–11*), preincubated in the absence (−) or presence of 10 nM CsA (*lanes 7* and *10*) or 1 μM CsA (*lanes 5, 8,* and *11*). GAPDH antisense riboprobe was hybridized with total RNA as an internal control. The results are representative of three independent experiments. *B*, schematic shows the deletion and/or mutant DSCR-1 promoter constructs. *C*, HUVEC were transiently transfected with the DSCR-1 (−1664/+83)-luc plasmid and exposed to 50 ng/ml VEGF, 1.5 units/ml thrombin, or 10 ng/ml TNF-α for 6 h in the absence (−) or presence of 1 μM CsA. The results show the mean and S.D. of luciferase light units (relative to untreated and minus CsA cells) obtained in triplicates from at least three independent experiments. *D* and *E*, HUVEC were transiently transfected with deletion and/or mutant constructs and exposed to 50 ng/ml VEGF or 1.5 units/ml thrombin for 6 h. Each plasmid was co-transfected with pRL-SV40 to normalize for transfection efficiency. Promoter activities were determined relative to the normalized activity from DSCR-1 (−1664/+83)-luc plasmid in untreated cells (*D*) or each untreated control (*E*). *F*, HUVEC were transiently transfected with $(NF\text{-}AT)_4$-TATA-luc plasmid and exposed to 50 ng/ml VEGF, 1.5 unit/ml thrombin, or 10 ng/ml TNF-α for 6 h. *G*, HUVEC were transiently co-transfected with DSCR-1 (−350/+83)-luc and GATA-2 (pMT_2-GATA2), constitutively active NF-ATx (pSRα-CANF-AT), or vector alone (pMT_2 or pSRα), alone or in combination. The means and S.D. values are derived from at least three separate experiments performed triplicate.

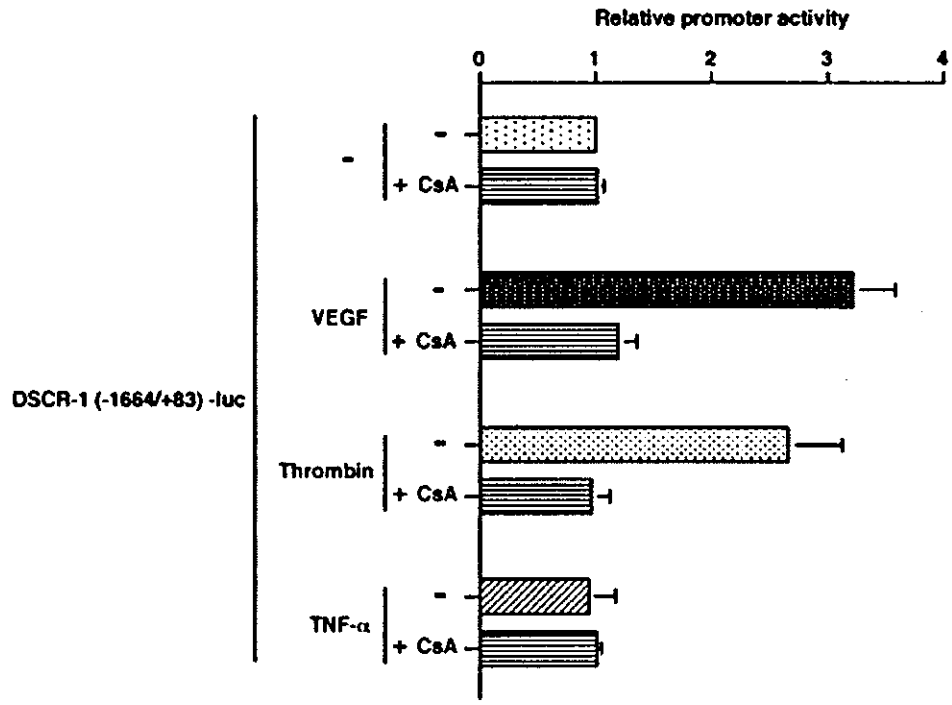

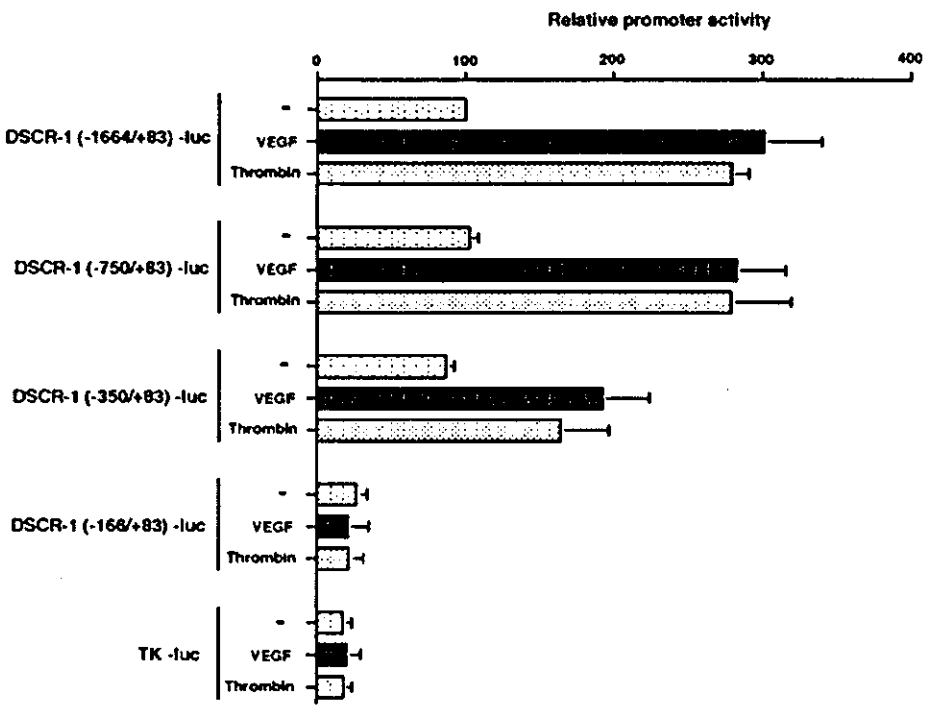

FIG. 4—*continued*

Tube Formation Assays—400-μl aliquots of type-I collagen gel (Koken, Tokyo, Japan) containing EGM-2-MV medium without basic fibroblast growth factor were used as described previously (22). Briefly, HUVEC infected with Ad-Control or Ad-DSCR-1 were seeded at 1×10^5 cells/well and incubated for 24 h in 5% CO_2. The medium was removed, and HUVEC were covered with 400 μl of the gel. Cells were incubated with 1 ml of EGM-2-MV medium in the absence of basic fibroblast growth factor. Two days later, a branched capillary network was visualized under a microscope. Images from at least three different areas in each well were captured by a digital camera under a microscope.

Matrigel Plug Assays—Matrigel (BD Biosciences) containing 50 ng of VEGF and either 10^9 plaque-forming units of Ad-Control, Ad-DSCR-1, or Ad-DSCR-1 plus Ad-CA-NFAT was injected subcutaneously into C57BL6 mice. After 14 days, matrigel plugs were removed for histological sections. Alternatively, the matrigel plugs were

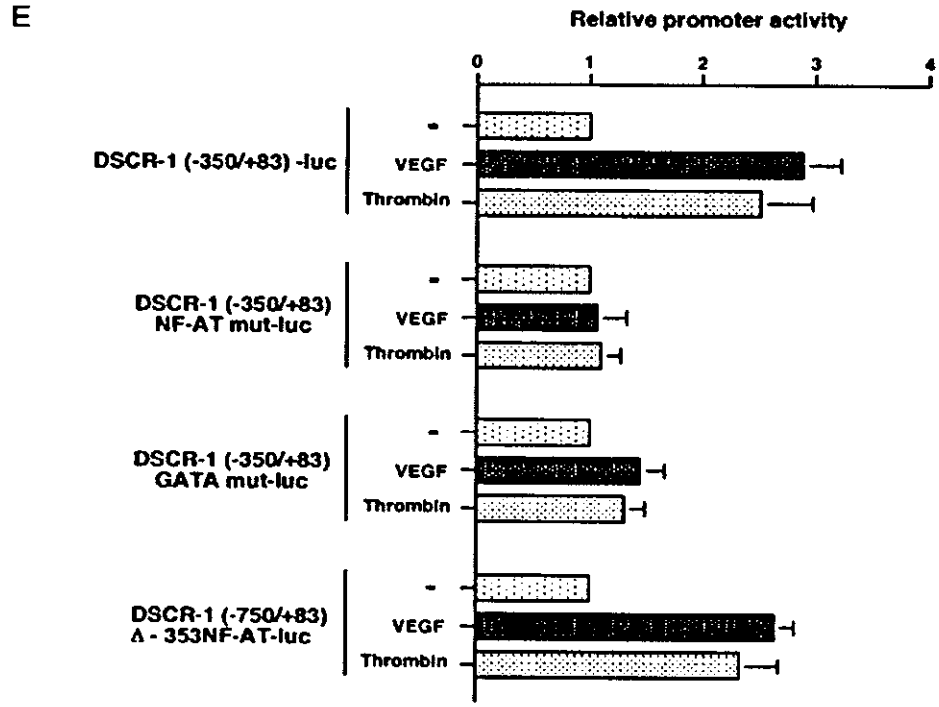

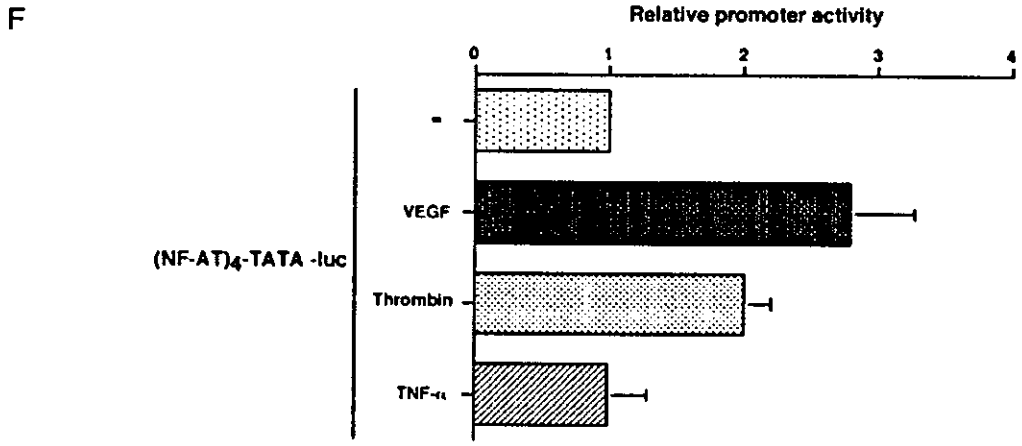

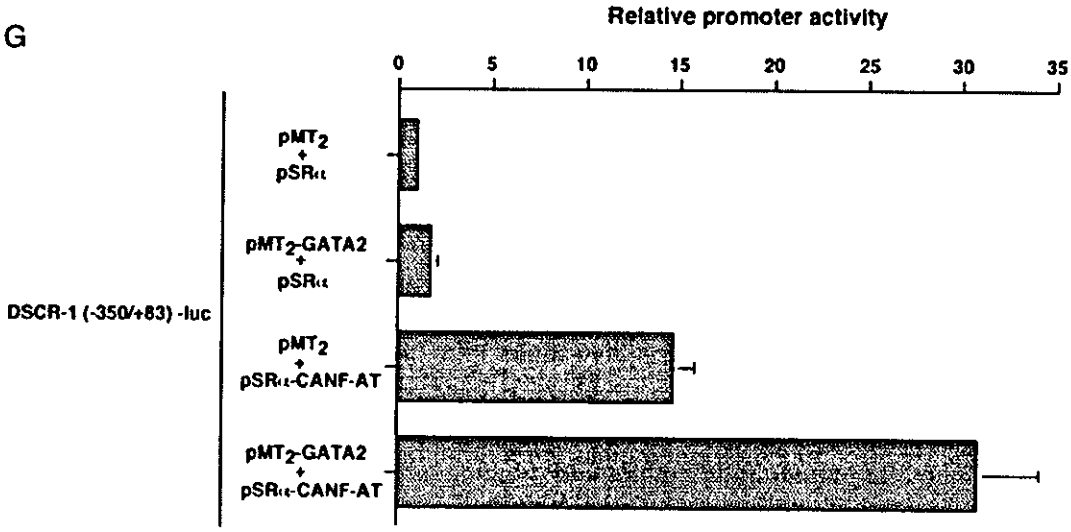

FIG. 4—*continued*

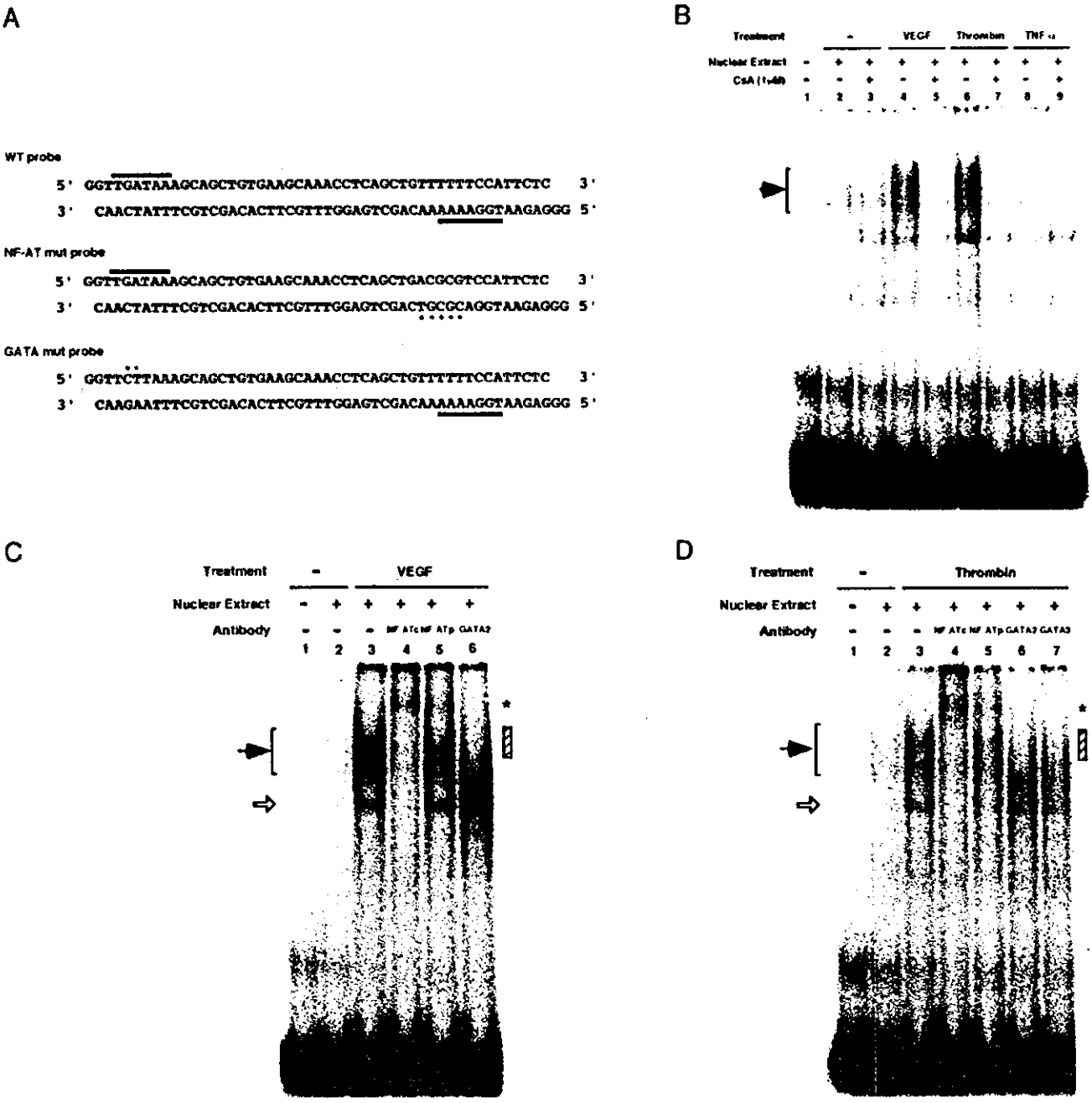

FIG. 5. **VEGF and thrombin response element on the DSCR-1 binds NF-ATc and NF-Atp and GATA-2 and -3.** *A*, schematic representation of the probe sequences used in EMSA. The consensus NF-AT and GATA motifs are *underlined*. The mutated bases are represented by *asterisks*. *B*, EMSAs were performed with ^{32}P-labeled WT probe and nuclear extract from untreated HUVEC (− treatment) (*lanes 2* and *3*) or HUVEC treated with 50 ng/ml VEGF (*lanes 4* and *5*), 1.5 units/ml thrombin (*lanes 6* and *7*), or 10 ng/ml TNF-α (*lanes 8* and *9*), in the absence (−) or presence (+) of 1 μM CsA. The *arrow* indicates the CsA-sensitive DNA-protein complexes. *C* and *D*, nuclear extracts from untreated (*lane 2*) and VEGF (*C*)- or thrombin (*D*)-treated HUVEC were incubated in the absence (*lanes 2* and *3*) or presence of antibodies against NF-ATc (*lane 4*), NF-ATp (*lane 5*), GATA-2 (*lane 6*), or GATA-3 (*D, lane 7*). The *asterisks* indicate the supershifted complex. The *hatched rectangles* indicate the inhibited complex. *E*, EMSAs were performed with ^{32}P-labeled NF-AT mutant probe in the absence (*lane 1*) or presence of nuclear extracts from VEGF-treated HUVEC, incubated without (*lane 2*) or with 100-fold molar excess of unlabeled NF-AT mutant (*lane 3, self*) GATA mutant (*lane 4, mut*) or antibodies against GATA-6 (*lane 5*), GATA-3 (*lane 6*), or GATA-2 (*lane 7*). *F*, EMSAs were performed with ^{32}P-labeled GATA mutant probe in the absence (*lane 1*) or presence of nuclear extracts from VEGF-treated HUVEC incubated without (*lane 2*) or with 100-fold molar excess of unlabeled GATA mutant (*lane 3, self*), NF-AT mutant (*lane 4, mut*) or antibodies against NF-ATc (*lane 5*) or NF-ATp (*lane 6*). The *asterisk* indicates the supershifted complex.

weighed and homogenized at 4 °C. The hemoglobin content was assayed with a Drabkin's reagent kit 525 (Sigma) according to the manufacturer's protocol.

Solid Tumor Model—1 × 10^6 logarithmically growing B16-melanoma cells were implanted subcutaneously into the right hind flank of C57BL6 mice. When the tumor reached about 50 mm^3 in volume, it was injected with 5 × 10^9 plaque-forming units of Ad-DSCR-1 or Ad-Control. Tumor volume (mm^3) was determined using length × width × height × 0.52 after caliper measurement.

RESULTS

DSCR-1 Is the Most Highly Induced Gene in VEGF- and Thrombin-treated Primary Human Endothelial Cells—Endo-

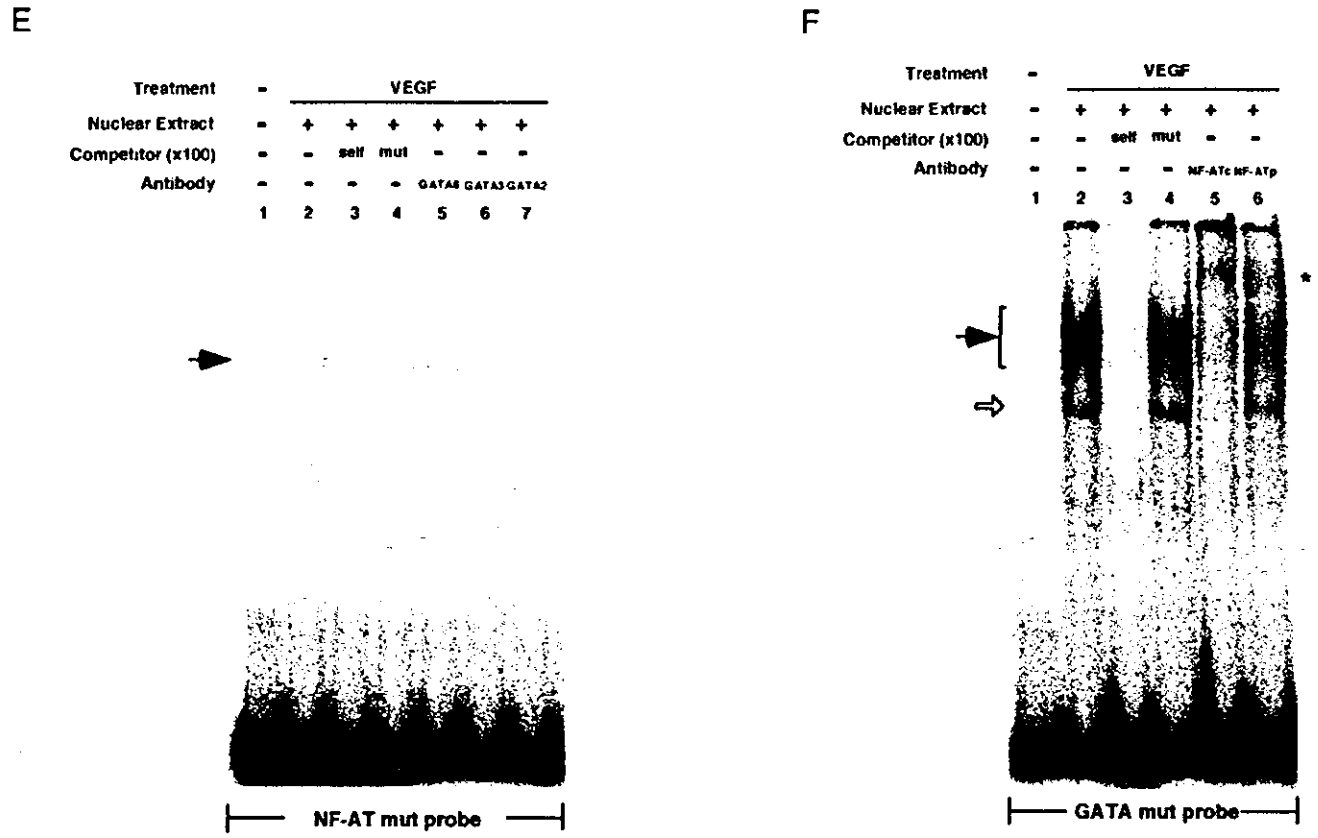

FIG. 5—*continued*

thelial cell activation is not an all-or-none response. Indeed, different extra-cellular mediators engage the endothelium in ways that differ from one signal to the next. A major focus is to study the temporal and spatial dynamics of endothelial cell phenotypes. Using DNA microarrays, we carried out a global survey of mRNA in HUVEC treated in the absence or presence of growth factor (VEGF), serine protease (thrombin), or cytokine (TNF-α). Clustering analyses of the data revealed a far closer relationship between VEGF and thrombin than between other pairings (Fig. 1*A* and supplemental Table I). Of the various transcripts that were responsive both to VEGF and thrombin, DSCR-1 was the most highly induced at the earliest time point. At 1 h, VEGF resulted in 22.3-fold induction of DSCR-1, while thrombin induced DSCR-1 by 17.7-fold (Fig. 1*B*). The effect of VEGF and thrombin was no longer detectable at 24 and 18 h, respectively. Compared with VEGF and thrombin, TNF-α treatment of HUVEC resulted in far less induction of DSCR-1 (3.2-fold at 1 h) (supplemental Table I and data not shown).

VEGF and Thrombin Selectively Induce the DSCR-1 Isoform Consisting of Exons 4–7 in Primary Human Endothelial Cells—The DSCR-1 gene includes seven exons and six introns. The first four exons are alternative and code for four different isoforms (23, 24). A 5′ promoter regulates expression of the first three isoforms, which are derived from alternative splicing. The most common of these contains exons 1, 5, 6, and 7. An intragenic region between exons 3 and 4 contains an alternative promoter which initiates transcription of the fourth isoform (exons 4, 5, 6, and 7) (Fig. 2*A*) (24). To determine which isoform(s) is up-regulated by VEGF and thrombin, we performed RNase protection assays using riboprobes that span either exons 4 and 5 or exons 1 and 5 (Fig. 2*B*). As shown in Fig. 2*C*, the addition of VEGF or thrombin to HUVEC resulted in marked up-regulation of the DSCR-1 isoform encoded by exons 4–7, with maximal levels occurring at 1 h. In contrast, there was no detectable induction of the DSCR-1 isoform encoded by exons 1, 5, 6 and 7 (Fig. 2*C*, *asterisk*). Consistent with the DNA microarray data, TNF-α resulted in comparatively low levels of DSCR-1 induction. To determine whether DSCR encoding exons 1, 5, 6, and 7 is expressed in endothelial cells and to further test its inducibility, RT-PCR assays were performed using isoform-specific primers and cDNA from control or VEGF-, thrombin-, or TNF-α-treated HUVEC. Transcripts were detected only after 40 cycles of amplification and were not affected by the addition of extracellular mediators at 1 or 4 h. By comparison, the isoform encoded by exons 4–7 was detected in thrombin- and VEGF-treated HUVEC after just 21 PCR cycles (Fig. 2*D*). Together, these results suggest VEGF and thrombin and to a far lesser extent TNF-α result in the rapid and selective induction of the DSCR-1 isoform containing exons 4–7.

VEGF and Thrombin Induce DSCR-1 Expression in Primary Human Endothelial Cells via Flk-1/KDR and PAR-1, Respectively—VEGF has two high affinity receptors, Flt-1 and Flk-1/KDR. To determine which receptor mediates VEGF stimulation of DSCR-1, HUVEC were treated with the selective Flt-1 agonist, PlGF, or with VEGF in the absence or presence of the Flk-1/KDR selective inhibitor, SU1498. The addition of 50–200 ng/ml PlGF failed to induce DSCR-1 mRNA (Fig. 3*A*, *lanes 2* and *3*). In contrast, VEGF-mediated induction of DSCR-1 was attenuated by pretreatment with 5 and 20 μM SU1498, by 74.2 and 84.4%, respectively (Fig. 3*A*, *lanes 4–6*). As an internal control for PlGF activity in HUVEC, agonist-treated endothelial cells were assayed for Flt-1 phosphorylation, using immunoprecipitation. As shown in Fig. 3*B*, the addition of 100 ng/ml PlGF resulted in tyrosine phosphorylation of Flt-1. Taken together, these data suggest that VEGF increases DSCR-1 mRNA in endothelial cells through a Flk-1/KDR-dependent mechanism.

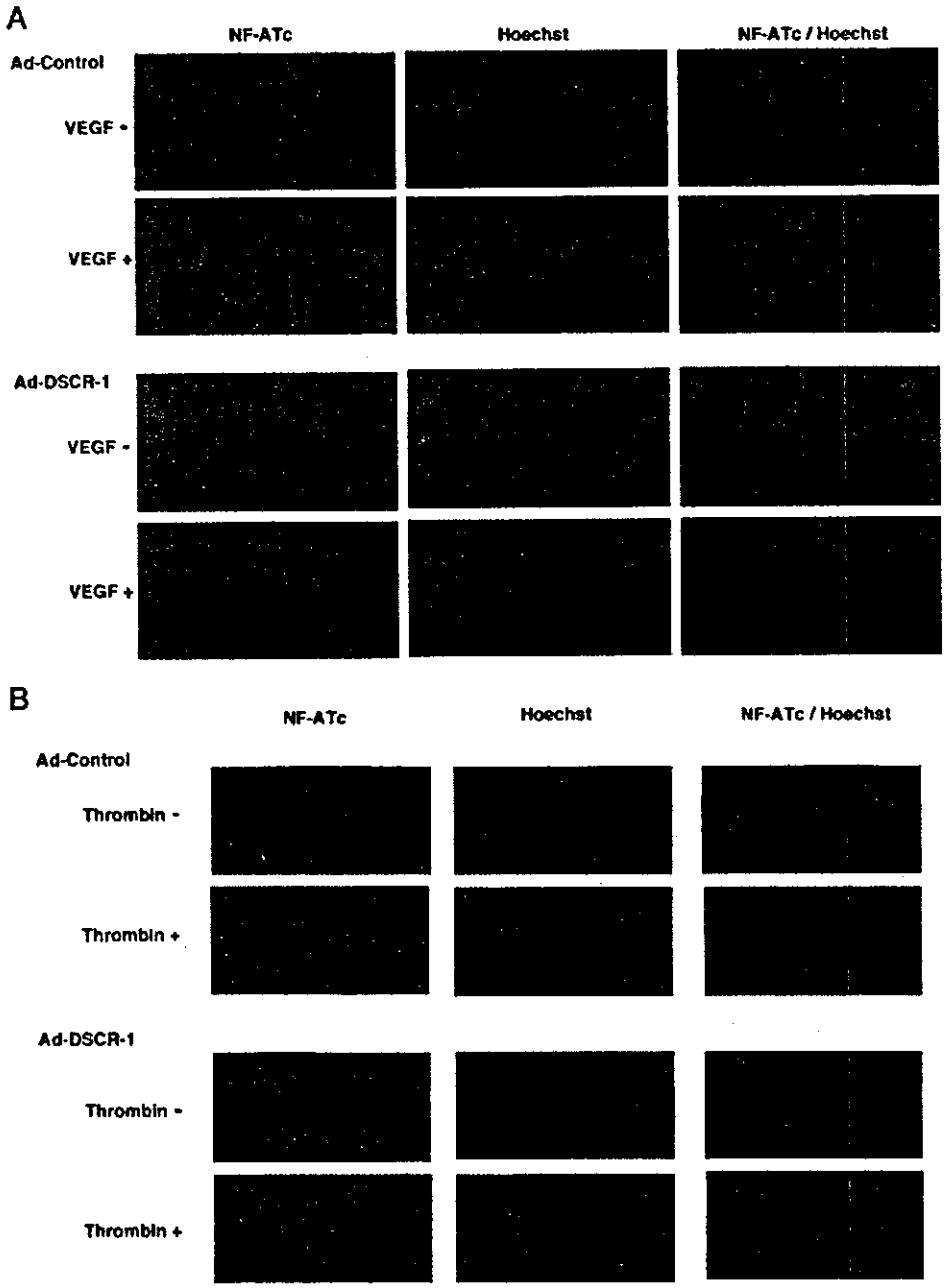

FIG. 6. **DSCR-1 attenuates tube formation and cell cycle progression of primary endothelial cells.** *A* and *B*, HUVEC were infected with either Ad-Control or Ad-DSCR-1 and then serum-starved for 18 h and incubated in the absence or presence of 50 ng/ml VEGF (*A*) or 1.5 units/ml thrombin (*B*) for 1 h. The nuclei were stained with Hoechst. *C*, capillary-like tube formation model. HUVEC were infected with either Ad-Control (*panels a–d*) or Ad-DSCR-1 (*panels e–h*), grown on the collagen gel in the presence (*panels b–d* and *f–h*) or absence (*panels a* and *d*) of VEGF. 48 h later, cells were observed under bright field (40-fold magnification (*panels a*, *b*, *e*, and *f*)) or under fluorescence (40-fold magnification (*panels c* and *g*) or 100-fold magnification (*panels d* and *h*)). The results are representative of three independent experiments. *D*, quantification of tube area. The means and S.D. values were calculated with NIH image from three independent experiments. *E*, FACS analysis of cell cycle in Ad-Control-, Ad-DSCR-1-, and Ad-DSCR-1 plus Ad-CA-NFAT-infected HUVEC, carried out as described under "Experimental Procedures." The results are representative of three independent experiments. *F*, FACS analysis of apoptosis and necrosis in Ad-Control- and Ad-DSCR-1-infected HUVEC: *panel a*, representative result showing M1 (G_1/G_0), M2 (G_2), M3 (S), and M4 (apoptosis and necrosis) fields; *panel b*, the percentage gated in each field.

Thrombin is known to signal through protease-activated receptors (PARs). PAR-1 is the most important thrombin receptor in endothelial cells. To demonstrate a potential role for PAR-1 in mediating the thrombin response, we employed RNase protection assays of HUVEC treated in the presence or absence of TRAP, a 14-amino acid PAR-1 agonist peptide. TRAP resulted in a dose-dependent increase in DSCR-1 mRNA levels. Moreover, thrombin-mediated induction of DSCR-1 was completely blocked by pretreatment with the thrombin-specific inhibitor, hirudin (Fig. 3, *C* and *D*). Taken together, these findings suggest that VEGF and thrombin mediate DSCR-1 induction in endothelial cells via Flk-1/KDR and PAR-1, respectively.

VEGF- and Thrombin-induced DSCR-1 mRNA and Promoter Activity in Primary Human Endothelial Cells via a Calcineurin-dependent Signaling Pathway—Previous studies in non-endothelial cells have demonstrated an important biological role for DSCR-1 as a regulator of calcium-calcineurin-NF-AT signaling (25–27). To determine whether VEGF- and

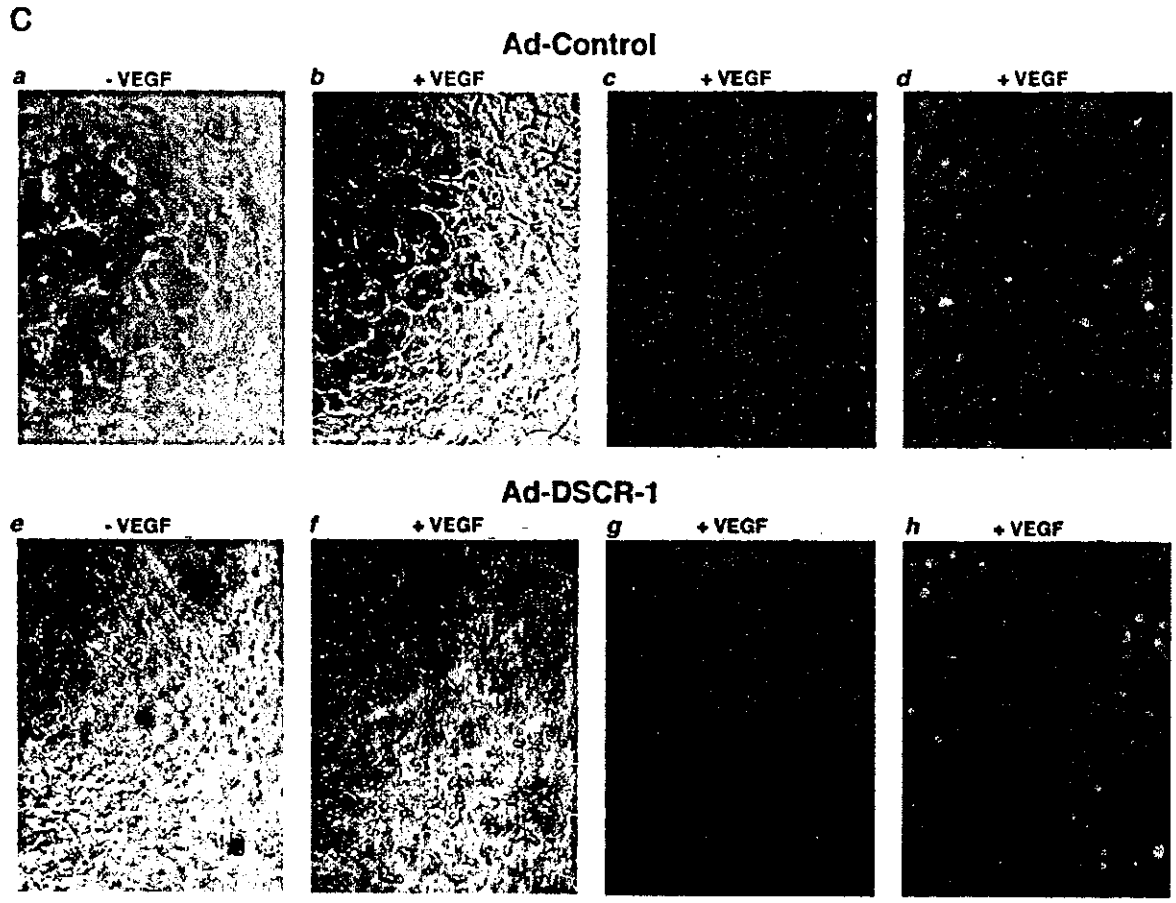

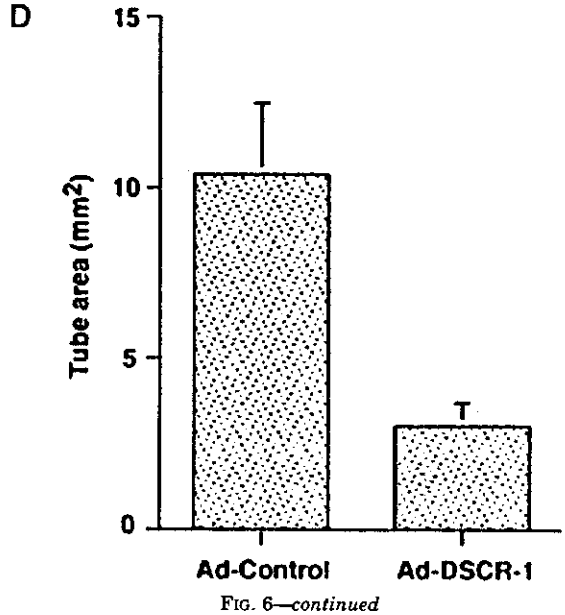

FIG. 6—*continued*

thrombin-mediated induction of DSCR-1 in endothelial cells is similarly dependent on calcineurin, we employed RNase protection assays with the calcineurin inhibitor, cyclosporine A (CsA). VEGF-mediated induction of DSCR-1 was inhibited 64.1% by 10 nM CsA and 93.3% by 1 μM CsA (Fig. 4*A*, *lanes 6–8*). Similarly, thrombin stimulation of DSCR-1 was inhibited by pretreatment with 10 nM and 1 μM CsA (by 72.6 and 93.1%, respectively) (Fig. 4*A*, *lanes 9–11*). Next, we wished to determine whether the DSCR-1 promoter contained information for transducing the VEGF/thrombin-calcineurin-dependent signal. To that end, the human DSCR-1 promoter (−1664 to +83) was isolated and coupled to the luciferase reporter gene (Fig. 4*B*). The resulting DSCR-1-luc plasmid was transiently transfected into HUVEC. As shown in Fig. 4*C*, VEGF and thrombin induced DSCR-1 promoter activity by 3.2- and 2.6-fold, respectively, whereas TNF-α had no such effect. VEGF- and throm-

E

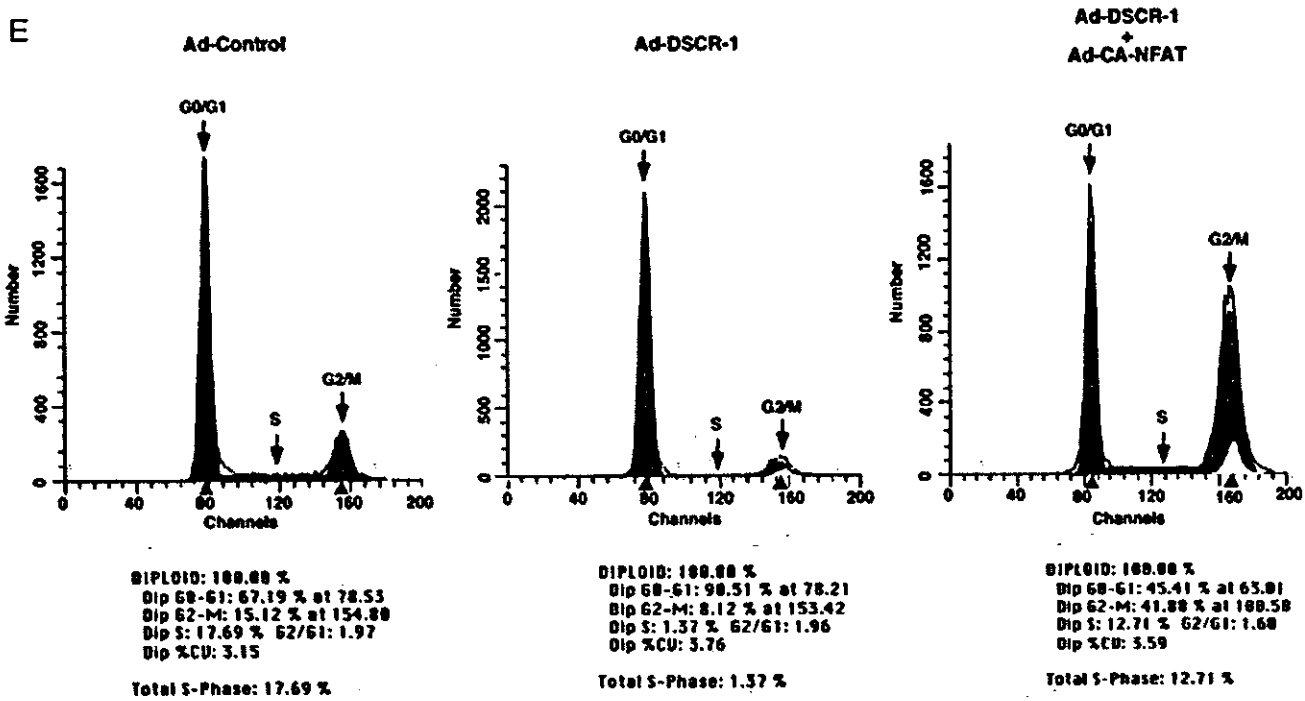

F

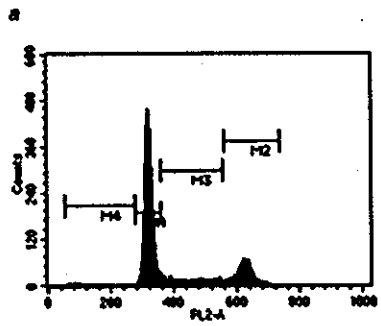

Ad-Control

1 st experiment		2 nd experiment	
Marker	% Gated	Marker	% Gated
M1	75.80	M1	67.57
M2	11.90	M2	20.60
M3	10.83	M3	11.28
M4	0.91	M4	0.68

Ad-DSCR-1

1 st experiment		2 nd experiment	
Marker	% Gated	Marker	% Gated
M1	90.20	M1	88.39
M2	7.49	M2	9.80
M3	0.81	M3	1.15
M4	1.50	M4	0.65

FIG. 6—*continued*

bin-mediated induction of the promoter was inhibited by 1 μM CsA (90.7 and 96.3%, respectively). Taken together, these results indicate that both VEGF-Flk-1/KDR and thrombin-PAR-1 signals induce DSCR-1 mRNA and promoter activity through a calcineurin-dependent pathway.

To delineate the promoter elements responsible for mediating the effects of VEGF and thrombin on DSCR-1 expression, a series of 5′-deletion constructs was generated and transiently transfected into HUVEC (Fig. 4*B*). Most notably, a deletion of the promoter region between −350/−166 resulted in a loss of response to VEGF and thrombin (Fig. 4*D*). The region contains neighboring consensus NF-AT and GATA motifs located at positions −220 and −254, respectively. To assess the role of each of these DNA elements in mediating VEGF and thrombin stimulation of DSCR-1, a point mutation of either the NF-AT or GATA motif was introduced and the resulting construct transfected into HUVEC. Each mutation profoundly blocked VEGF/thrombin-mediated the induction (Fig. 4, *E* and *F*). To test the capacity of NF-AT and GATA factors to transactivate the DSCR-1 promoter, we carried out co-transfections in HUVEC with DSCR-1-luc and NF-AT and/or GATA expression plasmids. As shown in Fig. 4*G*, co-transfection of constitutive active NF-AT resulted in marked transactivation of promoter activity (14.6-fold). Co-transfection of GATA-2 resulted in weak but significant induction of promoter activity (1.71-fold). Importantly, GATA-2 and NF-AT interacted synergistically to induce the promoter by 30.8-fold.

VEGF and Thrombin Promote Binding of NF-ATc, NF-ATp, GATA-2, and GATA-3 to the DSCR-1 Promoter—To study the effect of VEGF and thrombin on NF-AT and GATA DNA-protein interactions, we carried out EMSA using radiolabeled oligonucleotide probes that spanned one or both consensus motifs. In the first set of experiments, a radiolabeled wild-type probe, containing the closely aligned GATA and NF-AT binding sites (Fig. 5*A*), was incubated with nuclear extracts derived from HUVEC treated in the absence or presence of VEGF, thrombin, or TNF-α. In control untreated cells, EMSA revealed a specific DNA-protein complex (Fig. 5*B*, *arrow*). Importantly, the addition of VEGF or thrombin, but not TNF-α, resulted in marked increase the DNA binding activity, an effect that was abrogated by pretreatment of cells with 1 μM CsA (Fig. 5*B*, compare *lanes 4, 6, and 8* with *lanes 5, 7, and 9*). These DNA-protein complexes were inhibited by the addition of 100-fold molar excess of the unlabeled self-competitor, but not by the same concentration of the unlabeled NF-AT mutant competitor, or unlabeled GATA mutant competitor (supplemental Fig. 1).

To determine the identity of proteins in the VEGF- and

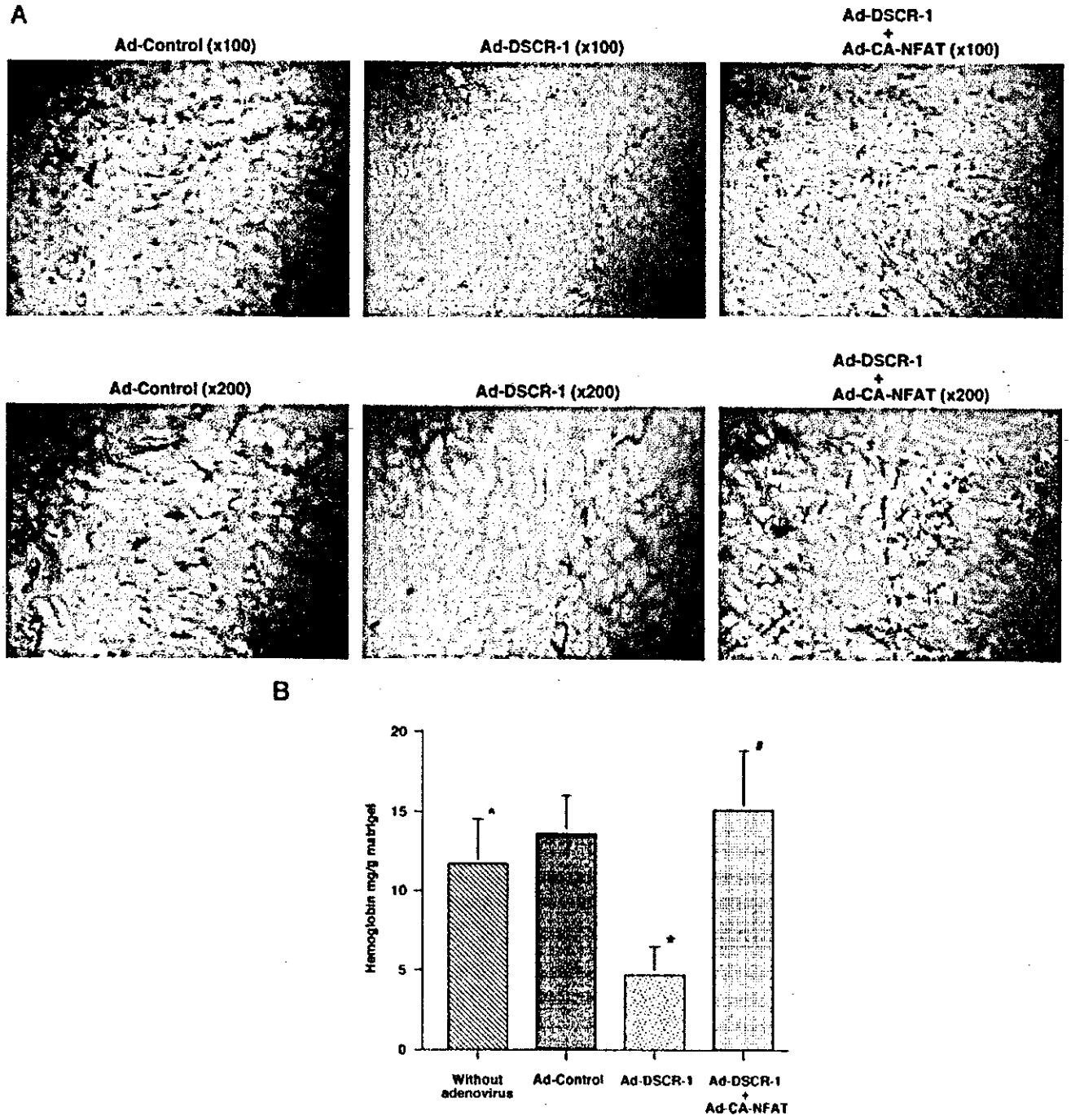

FIG. 7. **DSCR-1 attenuates matrix neo-vascularization and tumor-progression in mice.** *A*, matrigel containing 50 ng of VEGF and either 10^9 plaque-forming units of Ad-Control, Ad-DSCR-1, or Ad-DSCR-1 plus Ad-CA-NFAT was injected subcutaneously into C57BL6 mice. After 14 days, matrigel plugs were removed for analysis of new vessel formation by histological sections and hemoglobin assays. Optical magnifications were ×100 (*upper panels*) and ×200 (*lower panels*). The data are representative of seven independent experiments. *B*, hemoglobin in the matrigel plugs was measured using the Drabkin's reagents and normalized by the weight of matrigel. Data are expressed as means and S.D., $n = 5$. *, $p < 0.01$ compared with Ad-Control and Ad-DSCR-1. #, $p < 0.001$ compared with Ad-DSCR-1 and Ad-DSCR-1 and Ad-DSCR-1 plus Ad-CA-NFAT. [caret], $p > 0.5$ (not significant) compared with Ad-Control and uninfected control mice. *C*, DSCR-1 reduces B16-melanoma growth in mice. Tumor growth was reduced at 4 days (9.1-fold; $p < 0.04$), 6 days (7.7-fold; $p < 0.04$), and 8 days (7.4-fold; $p < 0.04$) by injection of Ad-DSCR-1. *D*, gross tumors representative of Ad-Control or Ad-DSCR-1 injected groups immediately after resection. *E*, tumor mass after 14 days following Ad-Control or Ad-DSCR-1 administrations. Data are expressed as means and S.D., $n = 5$. *, $p < 0.031$ compared with Ad-Control. *F*, representative sections of B16-melanoma at the edge (*panels a* and *c*) and center (*panels b* and *d*) of the tumor.

thrombin-inducible binding complex, the binding reactions were preincubated with anti-NF-ATc, anti-NF-ATp, anti-GATA-2, or anti-GATA-3 antibodies. The addition of an anti-NF-ATc antibody resulted in a strong supershift of the binding complex (Fig. 5, *C* and *D*, *lane 4*, *asterisks*), whereas anti-NF-ATp antibody resulted in a comparatively weak supershift (Fig. 5, *C* and *D*, *lane 5*). Preincubation with anti-GATA-2 or GATA-3 antibodies resulted in decreased intensity of DNA binding activity (Fig. 5*C*, *lane 6*, and *D*, *lanes 6* and *7*, *hatched rectangles*).

To more clearly assess GATA DNA-protein interactions, a radiolabeled probe containing the NF-AT mutant (Fig. 5A) was

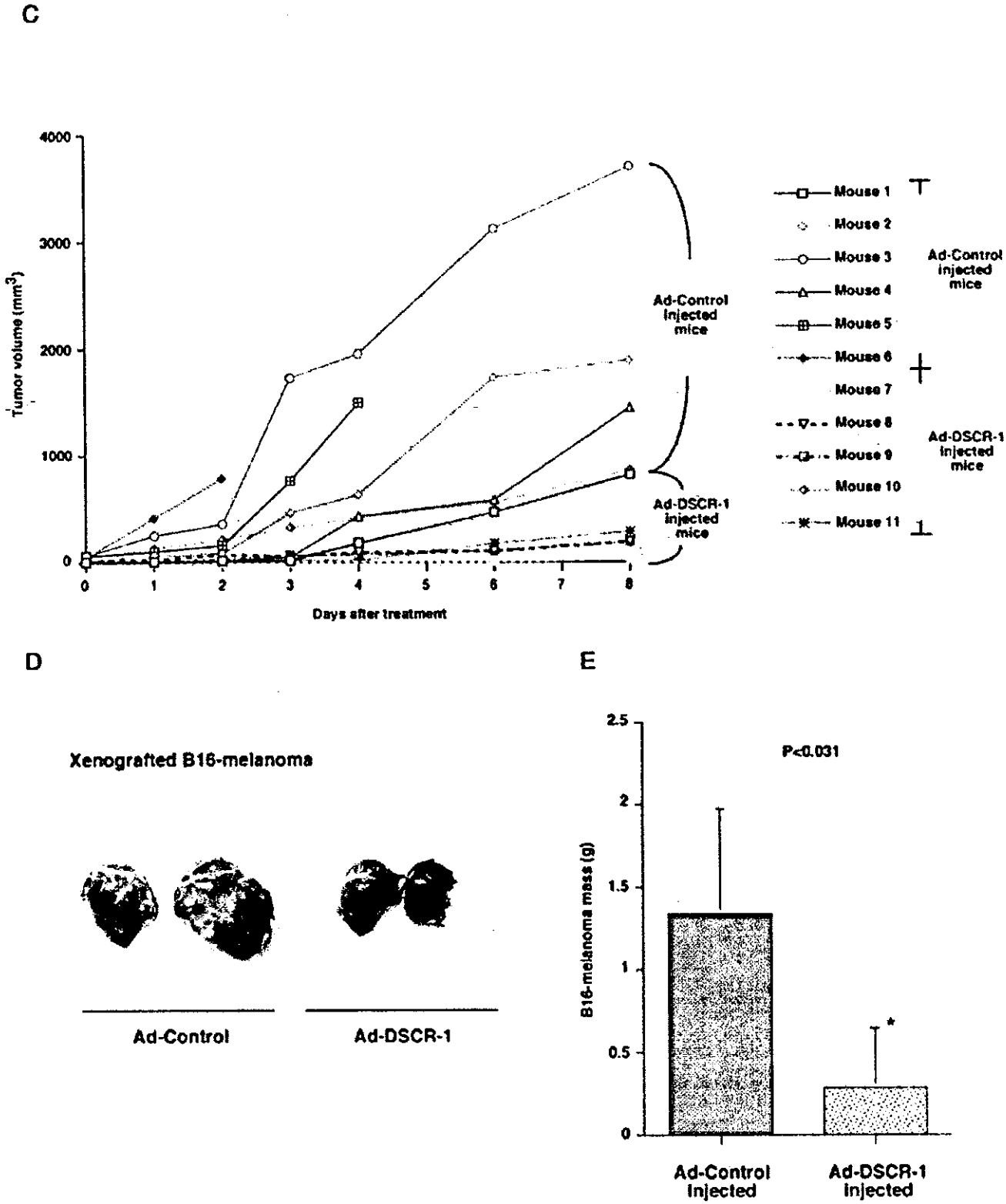

FIG. 7—*continued*

incubated with nuclear extracts derived from VEGF-treated HUVEC. These experiments resulted in specific DNA-protein complexes (Fig. 5*E*, *lane 2*, *arrow*), which were inhibited by the addition of 100-fold molar excess of unlabeled NF-AT mutant self-competitor but not inhibited by unlabeled GATA mutant competitor (Fig. 5*E*, *lanes 3* and *4*). Furthermore, the complexes were inhibited by preincubation with anti-GATA-2 or -3 antibodies but not by anti-GATA-6 antibody (Fig. 5*E*, *lanes 5–7*). To further study NF-AT binding, a radiolabeled probe containing the GATA mutant (Fig. 5*A*) was incubated with nuclear extracts derived from VEGF-treated HUVEC. The mixture resulted in a specific DNA-protein complex, which was